UNIVERSITAT POLITECNICA DE CATALUNYA

MASTER THESIS

Steady state cooling conditions of fast neutron source for BNCT therapy

Author:
Eng. Anna Talarowska

Supervisor:
Eng. Rafał Prokopowicz, PhD

A thesis submitted in fulfillment of the requirements
for the degree of Master in Nuclear Engineering

June 20, 2021

Declaration of Authorship

I, Anna Talarowska, declare that this thesis titled, "Steady state cooling conditions of fast neutron source for BNCT therapy" and the work presented in it are my own. I confirm that:

- This work was done wholly or mainly while in candidature for a research degree at this University.
- Where any part of this thesis has previously been submitted for a degree or any other qualification at this University or any other institution, this has been clearly stated.
- Where I have consulted the published work of others, this is always clearly attributed.
- Where I have quoted from the work of others, the source is always given. With the exception of such quotations, this thesis is entirely my own work.
- I have acknowledged all main sources of help.
- Where the thesis is based on work done by myself jointly with others, I have made clear exactly what was done by others and what I have contributed myself.

Signed:

Date:

Abstract

Anna Talarowska

Steady state cooling conditions of fast neutron source for BNCT therapy

Since 2001 the National Centre for Nuclear Research in Poland has been planning its BNCT test facility in Maria Research Reactor. The key issue is the beam quality needed to irradiate probes. For cellular cultures the thermal neutrons are optimal while for irradiating phantoms epithermal neutrons are required. Since the primary neutron energy spectrum from the reactor includes both fast neutrons and thermal ones, it is essential to shape the beam in a proper way. The beam will be based on two systems: neutron conversion system and the beam shaping system. The neutron conversion system is located on the periphery of the Maria reactor core and its main parts are uranium plates. Since the fission reaction occurs within plates the significant amount of heat is released that is why the proper cooling of the system has to be ensured.

So far only one BNCT facility has applied neutron conversion system; it was in Massachusetts Institute of Technology [Carpenter, 2012]. However, the converter in MIT was placed outside the reactor, which is not the case here in Świerk, Poland. In this thesis the cooling requirements and the safety limits are defined for neutron conversion system, by means of Computational Fluid Dynamics analysis of steady state thermal hydraulic performance of installation. The results presented in this thesis were used to determine whether the existing pool cooling conditions are suitable to ensure safe operation of the neutron converter. The applied initial and boundary conditions in the test cases cover the entire spectrum of NC operating conditions.

Acknowledgements

Firstly, I would like to send my gratitude to Michał Gryziński (Project director) for trust that such young person will manage the key safety issue of the project.

Secondly, I would like to thank Piotr Prusiński and Tomasz Kwiatkowski for sharing their experience in the CFD field, Rafał Prokopowicz and Mikołaj Tarchalski who were my supervisors while preparing the thesis for guiding me in writting and preparing the final content of the thesis whose help is invaluable.

Furthermore, I want to thank Lluis Batet Miracle for support during entire Master degree and Elisabet Mas de les Valls Ortiz, who introduced me to basics of CFD during lectures at UPC.

Finally, I would like to acknowledge NCBJ's and UPC's people, I have always been treated warmly and they always helped me as I required it.

Contents

List of Figures

List of Tables

List of Abbreviations

3D	three-**D**imesional
BC	**B**oundary **C**onditions
BNCT	**B**oron **N**eutron **C**apture **T**herapy
BSL	**B**a**s**e**l**ine
CFD	**C**omputational **F**luid **D**ynamics
CPU	**c**entral **p**rocessing **u**nit
FP	**F**uel **P**lates
MRR	**M**aria **R**esearch **R**eactor
NC	**N**eutron **C**onverter
NCBJ	**N**arodowe **C**entrum **B**adań **J**ądrowych (National Centre for Nuclear Research)
ONBR	**O**nset of **N**ucleate **B**oiling **R**atio
PCT	**P**eak **C**ladding **T**emperature
RANS	**R**eynolds-**A**veraged **N**avier-**S**tokes
RNG	**Re**normalization **G**roup
SbFP	**S**lots **b**etween **F**uel **P**lates
SST	**S**hear-**S**tress **T**ransport
STEP	**S**tandard **f**or **t**he **E**xchange of **P**roduct Model Data

List of Symbols

y^+	dimensionless distance to the wall	
u_τ	friction velocity, also called shear velocity	ms^{-1}
y	vertical distance normal to wall direction	m
ν	kinematic viscosity	m^2s^-1
k	turbulence kinetic energy	m^2/s^2
ω	specific dissipation rate	$1/s$
ϵ	turbulence energy dissipation rate	m^2/s^3
T_{ONB}	onset of nucleate boiling temperature	K
T_{sat}	saturation temperature	K
q	wall heat flux	W/m^2
p	water pressure	Pa
T_{in}	water temperature at the inlet to the channel	K
$T_{k,max}$	maximum wall temperature	K
Q	rate of heat transfer	W
h	heat transfer coefficient	W/m^2K
A_s	surface area	m^2
T_s	surface temperature	K
T_∞	bulk fluid temperature	K
$\frac{dT}{dx}$	temperature gradient	
R_{cond}	thermal resistance against conduction	m W/K
R_{conv}	thermal resistance against convection	m W/K

1 Introduction

The thesis is organized as follows: in the first chapter the background to this thesis is presented. In the second chapter research objectives are stated, a description of analyzed geometry and numerical model are given in Chapter 3; in Chapter 4 the calculation results are presented; in Chapter 5 the conclusions are drawn. In Appendix A the mesh influence on the results is studied, while Appendix B shows the turbulence model sensitivity study.

1.1 The MARIA Research Reactor characteristics

MARIA Research Reactor is a multi-purpose pool-type reactor with pressurized fuel elements in the core. Fuel elements contain concentric six-tube assemblies of fuel elements. It is a high flux reactor of 30MW nominal power moderated with water and beryllium. The thermal and fast neutron flux density may reach $3 * 10^{14} n/cm^2 s$ and $2 * 10^{14} n/cm^2 s$ respectively. The reactor has been designed with a high degree of application flexibility. Fuel channels are situated in the beryllium matrix enclosed by a lateral reflector made of aluminium canned graphite blocks. Maria is equipped with vertical channels for irradiation target materials, a rabbit system for short irradiations located near fuel channels. Eight horizontal channels (numerated H1-H8) enable the neutron beams outside the reactor pool, six of which are operable today. Figure 1.1 presents the vertical section of MARIA reactor pool and the horizontal channels.

The reactor core has a modular design and its core configuration is fitted to either production or research purposes. The first reactor criticality was in December 1974 and operated until 1985, when its modernization started. During the outage, which lasted until 1993, the upgrading and refurbishment of technological systems took place. The efficiency of the cooling system and ventilation was improved. Reflector graphite blocks were overlooked and the beryllium matrix was enlarged. The Chernobyl disaster changed the approach to reactor safety analysis. As a result, several safety systems were introduced, such as passive reflooding of fuel channels and horizontal channels construction enhancement. The reactor is continuously improving, especially considering safety issues and reactor operation program. The second step of upgrading was performed during regular maintenance. From 1996 to 2002, the heat exchangers, instrumentation and control system were replaced. The radiation protection system was upgraded and the fuel element integrity monitoring system was modernized [Krzysztoszek, 2013]. Up to 2000, the 80% U-235 enriched fuel was

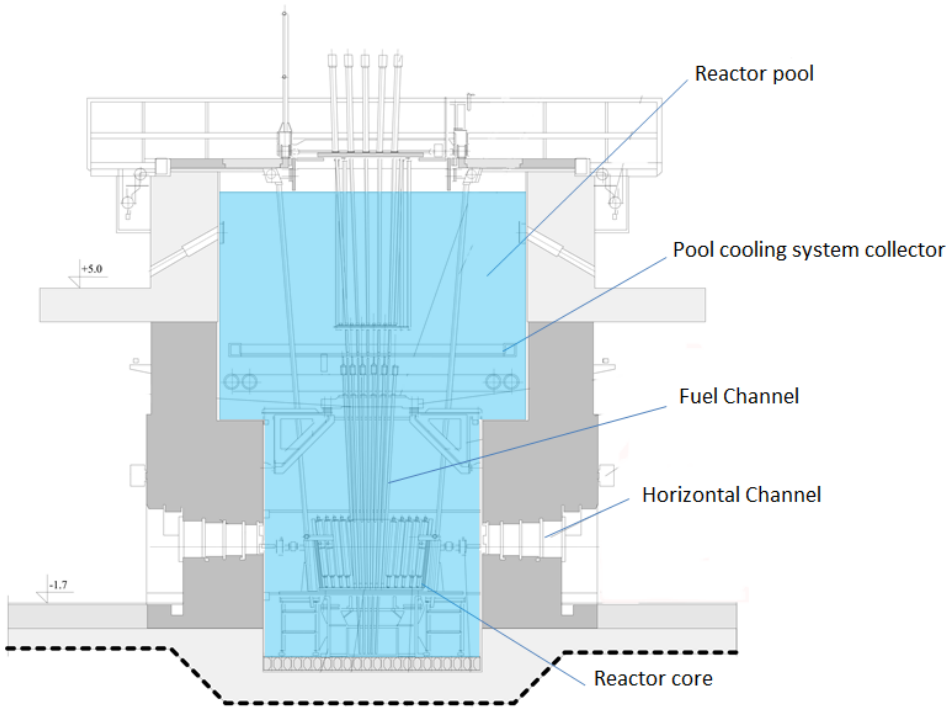

FIGURE 1.1: MARIA Reactor vertical section [K. Pytel, 2015].

used in MARIA. From the year 2000, the 36% enriched fuel elements were introduced to the core. Finally, in 2012 the 19.7% fuel enrichment was implemented and is used up to date. The change for 19.7% enriched fuel contributed to the primary cooling pumps replacement.

It is anticipated that MARIA will be able to operate until 2050 after several modernizations take place.

The MARIA Research reactor is a neutron source for irradiation of target materials for medicine and industry: radioisotope production, Mo-99 production, neutron modification of silicon doping and minerals. The main characteristics and operating data of MRR are presented in Table 1.1.

characteristic	value
nominal power	30 MWth
fast neutron flux	$2 * 10^{14} n/cm^2 s$
thermal neutron flux	$3 * 1014 n/cm^2 s$
fuel assemblies:	
- enrichment	19,7%
- cladding	aluminium
- shape	six concentric tubes
- active length	1000 mm
moderator	water, beryllium
fuel element	
- pressure	1.7 MW
- coolant flow	$30/25\ m^3/h$
- inlet temperature	10°C
- outlet temperature	110°C
maximum temperature in reactor pool	50°C
water volume	
- reactor pool	$250m^3$
- cooling circuit	$20m^3$
nominal pool water level	7.05 m
reactor core center level	-0.55 m

TABLE 1.1: MARIA Reactor data [Krzysztoszek, 2016].

1.2 Boron Neutron Capture Therapy

Boron Neutron Capture Therapy is an experimental radiotherapy technique that enables treatment of malicious tumours, especially head and neck cancers, which do not give anticipated results during other types of therapy. Advantages of BNCT therapy are enumerated in IAEA-TECDOC-1223, 2001. In addition, it is worth mentioning non-toxicity of boron compounds concentrated in tissue, possible time interval optimization to maximize therapeutic effect and the fact that the therapy effects are observable on the cellular level. Therapy is based on the thermal neutron capture by boron nucleus (Figure 1.2):

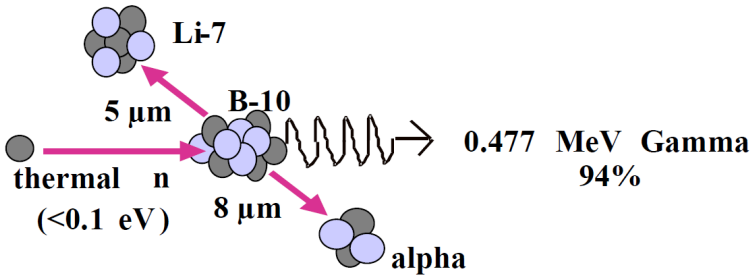

FIGURE 1.2: Neutron capture - basis for BCNT therapy [IAEA-TECDOC-1223, 2001].

Initially, a boron compound with the highest affinity to the tumor cell other than a healthy one, is administered to a patient through intravenous infusion. In the next

step of the BNCT therapy tumor is irradiated by neutrons which energy is fitted according to the tumor location. Neutrons lose their energy with distance and become thermal as they approach diseased tissue. As the boron nuclei absorbs neutron, the reaction takes place producing two heavy particles that dissipate their energy in a single cell which is damaged.

The recommended thermal neutron fluence which should be delivered to diseased tissue and the boron concentration in tumour (for glioblastoma multiform) equals to $5 * 10^{12}\ n/cm^2$ and $44 - 93\ mg/g$ respectively [H. Koivunoroa, 2015]. The epithermal neutron beam is considered to be optimal for treatment since neutrons of such energies thermalize in tissue at 2.0 cm depth (See Figure 1.3). As a result, such the beam enables maximizing thermal neutron flux density delivery to a tumor while minimizing radiation dose to healthy tissues.

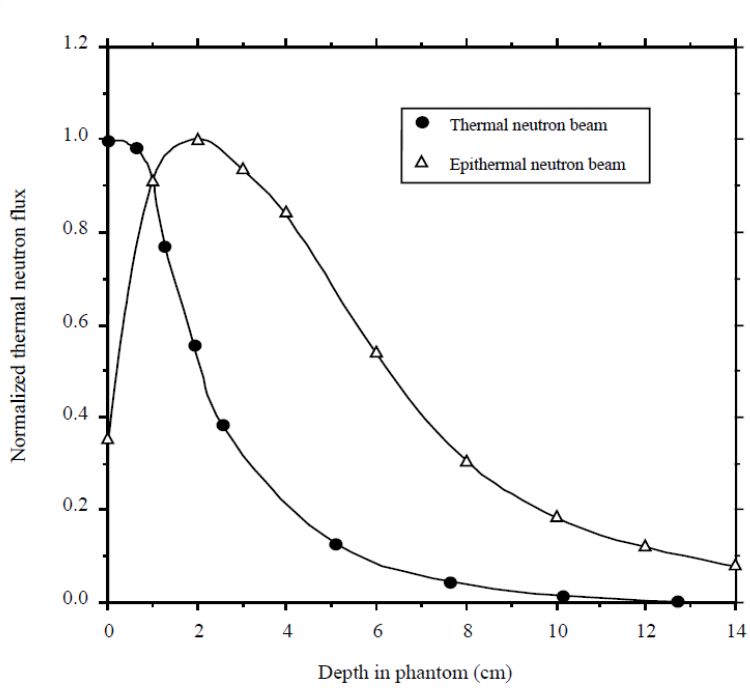

FIGURE 1.3: Comparison of flux distribution according to beam energy [IAEA-TECDOC-1223, 2001].

1.3 BNCT Test Facility at H2 Channel

Neutron flux for BNCT may be received from fission reactions placed in the centre of the reactor core. Due to the peripheral location of BNCT facility, the density of this flux becomes low and well thermalized. This means that most of the neutrons are lost before they reach the desired location. The solution for this may be an implementation of neutron converter proposed by H .Rief, 1993 and it was applied successfully at Massachusetts Institute of Technology Nuclear Research Reactor, MITR

[O.K. Harling, 2002]. Using such a method, it is possible to obtain satisfactory neutron flux density in the desired energy spectrum. However, constructing a neutron converter is an issue at MARIA Reactor since existing infrastructure did not take into account such a possibility. The test facility, where pre-clinical medical studies for BNCT therapy will take place, is designed in front of the H2 horizontal channel exit. The research facility consists of an irradiation room, a preparation room and a control room. The visualization is shown in the Figure 1.4.

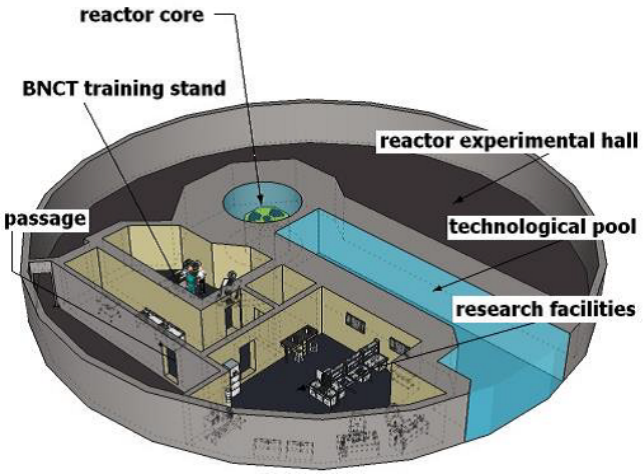

FIGURE 1.4: Training facility at MRR [M.A. Gryzinski, 2015].

The neutron spectrum measurements at the H2 channel exit revealed that the main components of the flux are thermal neutrons ($3 * 10^9$ n/cm^2s at channel exit). The thermal neutrons do not fulfil the requirements for boron neutron capture therapy. To meet the requirements of BNCT neutron beam a dedicated installation was designed. Its main components are uranium fuel plates, intermediate channel, a system of filters and collimator. The neutron beam from the centre of the reactor core will initiate a fission reaction in the converter. Fast neutrons produced in fuel plates inside converter will then go through moderator, filters and collimator to received finally expected neutron flux characteristic. The neutron converter and the intermediate channel are located in-pool while the remaining part is situated in the wall of the reactor pool. The installation scheme is presented in figure 1.5.

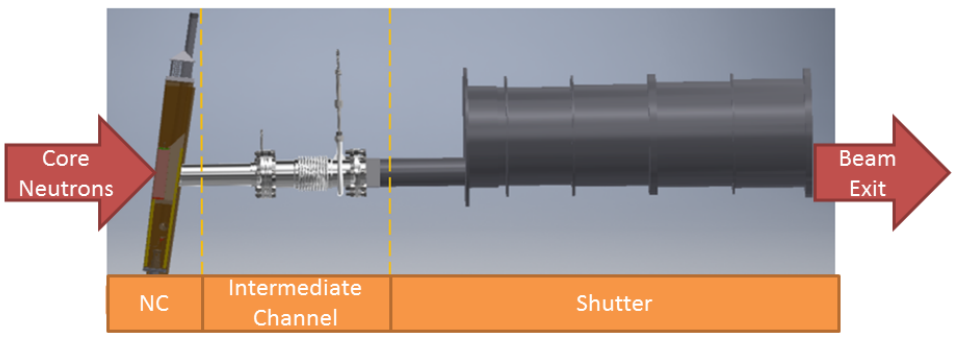

FIGURE 1.5: The H2 horizontal channel construction [Courtesy of G. Wojtania].

1.4 Neutrons Characteristics

The design of the neutron converter is based on primary core particles interaction with converter matter. The heat generation assists neutron interactions with matter. Fission and neutron capture reactions with neutrons slowing down are dominant heat sources in the reactor. According to Madland, 2006 those reactions may deliver 90% of total heat. The rest 10% is delivered by means of photon interactions with minor contributions of electrons and positrons interactions [Tarchalski, 2016]. To determine cooling conditions for the installation the spatial distribution of the heat generation has to be defined [J.R. Lamarsh, 2001].

In principle, the fission reaction in the uranium core of the Fuel Plate is responsible for the heat generation in the neutron converter.

Fission is a two-step process. The first step begins with high energy fission products, prompt fission neutrons and prompt fission gammas emission. Next, delayed fission products are released: neutrons, gammas, charged particles form fission products and neutron activated materials. U-235 fission releases around 200 MeV energy which is distributed by fission products. According to Prokopowicz, 2013 and Tarchalski, 2016 roughly 10% of heat is deposited outside the fuel assembly, mostly γ heating. The spatial distribution of the heat produced within the converter structure was determined with MCNP5 code, where neutron and gamma contribution was taken into account.

1.5 Neutron Conversion System

A neutron conversion system also called a neutron converter or converter is an integral part of the BNCT test facility placed in the MARIA research reactor. The centre of the neutron converter is made up of 24 fuel plates with uranium 235. The general idea of converter operation is to use neutron flux (origin from core centre) to initiate new fission reactions of U-235 in converter fuel plates. This results in fast neutrons release and it will be a fast neutron source for irradiation tests. The system is subcritical, which means that a self-sustaining reaction may not occur in any conceivable situation. This ensures the safety of this solution. Nonetheless, this installation will be a significant source of heat due to the fission reaction in it. For that reason, this converter needs formal approval from the Regulatory Body to be installed in the reactor core. There are several requirements that should be considered at the design stage to obtain consent to operation:

- specific cooling conditions have to be ensured,
- cooling of the reactor core should remain undisturbed,
- neutron distribution in the reactor core should remain unchanged.

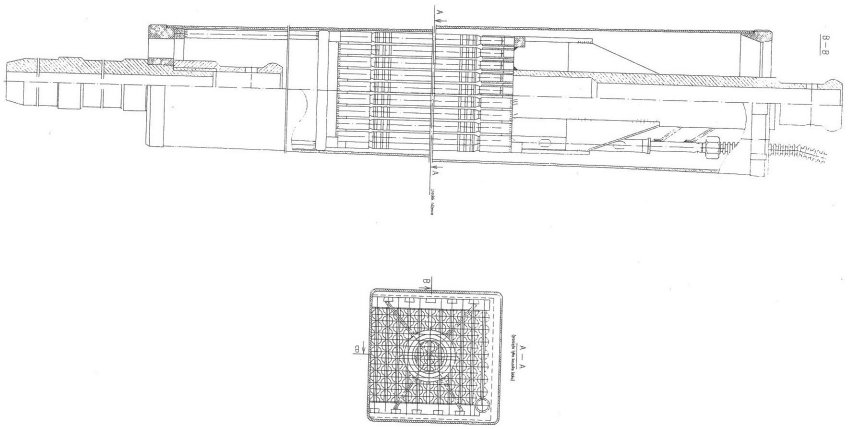

FIGURE 1.6: First neutron converter design [K. Pytel, 2010].

The neutron converter concept was analyzed in the Institute of Nuclear Physics in Kraków, where neutron and gamma simulation studies were performed. The details of the neutronic analysis are presented in the PhD thesis of Tracz, 2007. The converter is going to be located in the periphery of the reactor core, in the seat B-IV, replacing the graphite block. This location is also the nearest location to the H2 channel. In that configuration, thermal neutrons initiate fission reaction in the uranium core of the converter, which results in fast neutron production. The centre of the uranium core is located on the channel H2 axis, to increase the neutrons produced in the converter enter to the channel (fig. 1.11).

The converter outer dimensions are identical to the graphite block. It is shaped like an elongated truncated pyramid with a square base and constrictive downwards. A top and bottom separators welded to aluminium sleeve enable pool water to flow between the core blocks via a 1.5 mm gap (Bykowski, 1996).

1.5.1 First Design of neutron converter

The very first concept assumed to use of 98 EK-10 fuel rods and a measurement probe placed in a hexagonal lattice. The rods consist of U-235 10% enriched and aluminium cladding. Other converter components were made of aluminium. Since the fuel rods were stored for over 45 years, the clad integrity had to be tested. During the pumping method test 104 out of 120 rods appeared leak-proof. The CFD analysis showed that the proposed design was inappropriate as the significant bypass occurred in the periphery of the hexagonal lattice, which affects cooling within the central rods. The details of the mentioned analysis are presented in the article of P.A. Prusinski, 2012. Furthermore, some doubts on chemical composition occurred due to the long time storage of the fresh fuel. Hence, the new concept with fuel plates was designed.

1.5.2 Current Design of neutron converter

The converter core consists of two sets with 12 uranium plates each. Each plate is made up with pressed U-235, which is coated with aluminium. The uranium core of the plate measures 1.4 mm deep, 40 mm wide and 200 mm long. The total plate dimensions are 2.8 mm deep, 54 mm wide and 280 mm long which gives 40 mm aluminium at the top and the bottom of the uranium plate and 0.7 mm aluminium sheet on the sides (See Figure 1.7). The inner structure on the top of the baskets consists of a handle, a holding wire (spring) and a frame (marked green in the fig.1.8). The frame locks FP and the spring secures from sliding out of the set.

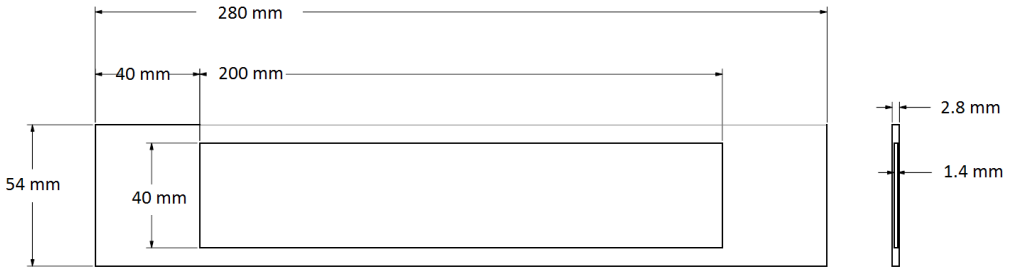

FIGURE 1.7: Fuel plate dimensions. Please note that the presented drawing is scaled for illustration purposes.

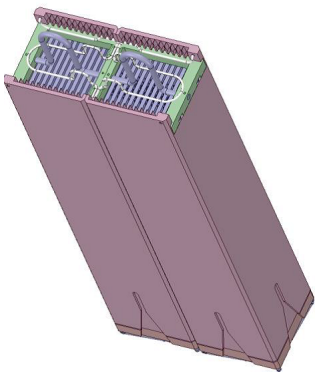

FIGURE 1.8: Top view of sets with uranium plates [Courtesy of Ł. Krzemiski].

The sets will be placed on the bearer inside the structure based on the original graphite block. The structure consists of cladding, filter, two side chocks, a curved aluminium block and a bearer mounted to the block and a leg (See Figure 1.9). The coolant enters the converter via filter above the sets blocks. Then, coolant flow is choked in a throat and stabilizes in rectangular slots. Next, water passes through the bearer with spring and finally, it is distributed into 26 rectangular slots between fuel plates. The slots are 48 mm wide and from 1.3 mm to 1.6 mm deep. Then the coolant enters the space below the plates where it mixes and leaves the rig via orifices in the base plate and leg. The flow diagram is shown in the figure 1.10.

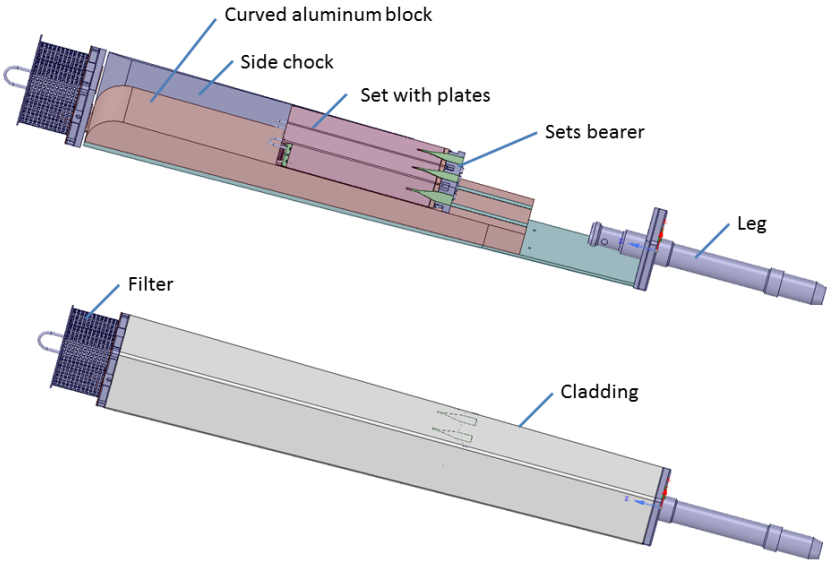

FIGURE 1.9: Top: Converter inner structure Bottom: Isometric view of converter sleeve [Courtesy of Ł. Krzemiski].

The converter will be placed in the periphery of the MARIA reactor core in place B-IV (Figure 1.11) instead of a graphite block. Since the reactor core is shaped like a truncated pyramid, the axis of external block is significantly deviated from a vertical axis. The converter axis is tilted from vertical by ca. 9 degrees. That is why the impact of gravity vector to flow distribution was investigated.

The baskets with plates face the reactor core, and they are oriented to the H2 channel axis. The half-height of the plates meet the H2 channel axis. The plates are oriented perpendicularly to the channel inlet, which is for better characteristics of neutrons in the H2 channel. The beam used for future tests will be shaped by a set of filters. Since the plates are located diagonally to the reactor core centre, the thermal neutron distribution reaching the converter is non-uniform. Consequently, the fission reaction rate will not be the same in all plates resulting in different heat load in each plate. The neutronic characterization and heat generation within the fuel plates were modelled with Monte Carlo code. The most loaded place is anticipated on the edge of the fuel plate, on the plate core edge, which is the nearest reactor core. Cooling of the converter can be done a either with reactor pool cooling or with dedicated cooling circuit. Specific cooling conditions determination for neutron converter is examined in this thesis.

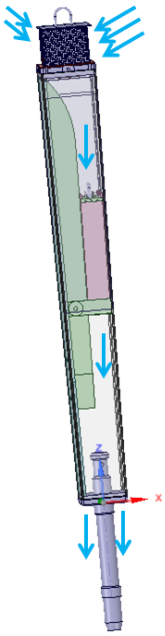

FIGURE 1.10: Coolant flow through the NC.

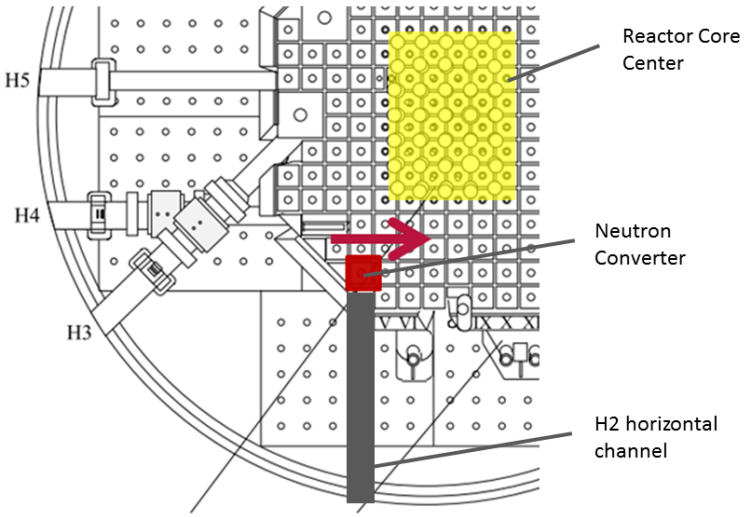

FIGURE 1.11: Location of the neutron converter [K. Pytel, 2015].

1.5.3 Heat transfer mechanisms

In section 1.4 the origin of heat generation in Fuel Plates was described, in this section the heat transfer mechanisms are presented with focus on the ones appearing in Neutron Converter. Heat transfer occurs as a result of temperature difference and the energy is always transported from a medium of higher temperature to the one with lower temperature [Cengel, 2012]. Three modes of heat transfer are defined: conduction, convection and radiation.

Conduction takes place in solids, liquids and gases as a result of particles collisions or diffusion during random motion. Convection occurs between solid and fluid on the boundary of the phases. This mode of heat transfer includes joined effect of fluid flow and conduction. The faster the fluid motion, the greater the convection heat transfer [Cengel, 2012]. Radiation is energy transport via electromagnetic waves (photons); thermal radiation is the energy emitted by bodies because of their temperature. All the bodies which temperature is above absolute zero emit thermal radiation.

Having considered operating conditions of Neutron Converter the dominant heat transfer mode is forced convection as the fluid flow is forced either by the pump of autonomous cooling system or the suction pumps of pool cooling system. Forced convection heat transfer rate is described by Newton's law (Equation 1.1).

$$Q_{conv} = hA_s(T_s - T_\infty) \tag{1.1}$$

Conduction occurs between uranium core and aluminium coating of fuel plate. The rate of heat transported in conduction mode is described by Fourier's law of conduction [Equation 1.2].

$$Q_{cond} = hA\frac{dT}{dx} \tag{1.2}$$

Equation 1.1 can be rearranged as:

$$Q_{cond} = \frac{T_1 - T_2}{R_{wall}} \tag{1.3}$$

where

$$R_{wall} = \frac{L}{hA} \tag{1.4}$$

Equation 1.4 describes conduction resistance of the wall which depend on geometry and thermal properties of the wall. Likewise Equation 1.2

$$Q_{conv} = \frac{T_1 - T_2}{R_{conv}} \tag{1.5}$$

where

$$R_{conv} = \frac{1}{hA} \tag{1.6}$$

Equation 1.6 describes convection resistance of the surface against convection which depends on convection heat transfer coefficient. Total thermal resistance is defined

as the sum of the thermal resistances against specific modes of heat transfer. For neutron converter it would be an aluminium wall resistance against conduction and convection resistance 1.7.

$$R_{total} = R_{cond} + R_{conv} = \frac{L}{kA} + \frac{1}{hA} \tag{1.7}$$

Both components of total thermal resistance depend on the surface area. It is a common practice to mount fins in order to increase the heat transfer area. The fins are made of highly conductive materials such as aluminium. In principle no heat generation occurs in the fins. Fuel plate has a 4 cm fin at its top and its bottom.

1.5.4 Onset of Nucleate Boiling Ratio

According to the K. Pytel, 2015 the minimum ONBR value for installation used in the MARIA reactor is 1.2. Having considered the results obtained with CFD analysis, the ONBR values was calculated. According to Foster-Greif Criteria [K.E. Forster, 1959]:

$$T_{ONB} = T_{sat} + 0,182\frac{q^{0,35}}{p^{0,35}} \tag{1.8}$$

$$ONBR = \frac{T_{ONB} - T_{in}}{T_{k,max} - T_{in}} \tag{1.9}$$

ONBR is a safety parameter that is studied to determine how far is the flow from the start of nucleate boiling (Point A at the fig. 1.12). There are two boiling crisis, both located on boiling curve one at the top of the left peak and the other at the right-hand side peak presented in the figure 1.12. The figure 1.12 shows the boiling curve for water at 1 atm where four boiling regimes are presented: natural convection boiling (Point A on the fig. 1.12), nucleate boiling (between points A-C), transition boiling (between points C-D) and film boiling (beyond point D).

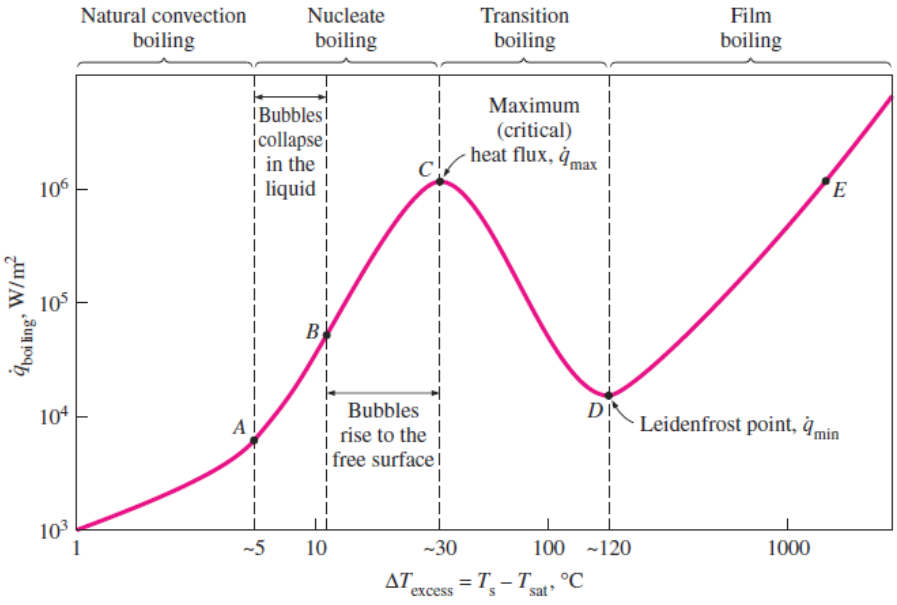

FIGURE 1.12: Typical boiling curve for water at 1 atm pressure [Cengel, 2012]

1.5.5 Flow contraction effect

Fuel plates act as an obstacle for the flow; the hydraulic diameter goes down from almost 80 mm to set of 26 rectangular slots of about 2.7 mm each. The geometric constriction causes eddies at the slots inlets, as it is depicted in the figure 1.13. There are several works that deal with eddies generation due to geometry changes [Abu-Mulaweh, 2004],[M.J. Sherry, 2009], [M. Ariff, 2009a], [M. Yaghoubi, 2004],[A.Sh. Kherbeet, 2016]. Having considered the geometry of the set, two basic geometries are identified blunt plates array and the backward facing step.

The frame which keeps FPs in place narrows down the inlet to the SbFP, creating a backward facing step, which causes flow separation and reattachment. The topic of backward facing step modelling [fig. 1.14] was analyzed in plenty of articles, also by M. Ariff, 2009b who used commercially available code to study the availability of the turbulence models implemented in the code to deal with complex flow structures.

J.C. Lane, 1980 underlines the importance of understanding the phenomena occurring at flat plate as it is *prototype for many heat transfer surfaces*, especially organized in an array. Although the theoretical and experimental studies on basic geometries seem to be well recognized, it was hardly possible to find a proper database to validate the results obtained in this thesis. The plates are located very closely and the plate width is almost double-size than the slot so a slot-width factor seems to play a significant role in flow development within each SbFP (A.S. Alzwayi, 2013). Neither converter plate nor channel can be analyzed alone in the preliminary study as the boundary conditions are unknown in that plates. In addition, water enters extreme and middle slots at significant angles which boost eddies generation. Since

eddies may affect the heat transfer conditions, the dimensions of generated eddies were investigated.

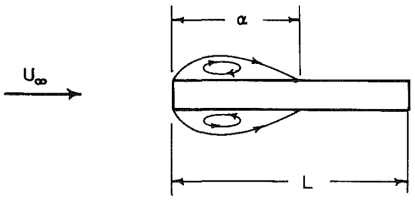

FIGURE 1.13: Eddies generation on the blunt plate [J.C. Lane, 1980].

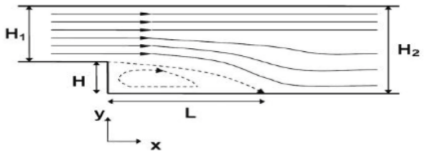

FIGURE 1.14: Backward facing step geometry and flow pattern [D.G. Jehad, 2015].

2 Research Objectives

The MRR pool cooling system capacity should be sufficient to ensure the safe operation of neutron converter in steady state operation. In order to prove the hypothesis, the cooling requirements for neutron converter have to be identified. The specific objectives and scope of research are as follows:

- To determine flow characteristic in the entire converter
- To determine the effect of coolant flow blockage at the inlet to the plate zones
- To determine minimal flow domain
- To calculate the level of heat transfer between the uranium plates

To achieve the primary objectives, numerical techniques were applied. The turbulence models available in ANSYS Fluent were applied to investigate the effect of blockage. The numerical model was used to determine whether the MARIA pool cooling would be enough to ensure safe operation of the converter. The parameters of interest are:

- Coolant mass flow distribution among the SbFP,
- Maximum and average velocity of the fluid
- Maximum temperature of the plate wall surface,
- Difference in the coolant temperature at the inlet and outlet to the channel

The presented work is focused on thermal hydraulic performance during steady-state operation of the installation which is going to be immersed in the reactor basket of Maria research reactor. The transient situation such as reactor power peak and loss of flow scenarios are going to be analysed after the validation test on the out-of the core hydraulic test stand, which is under construction at the time of the thesis defence. Moreover, the shorter geometry limited to plates and channels are planned for the transient calculations to shorten the computation time.

3 Methodology

Having considered the location, operating conditions and complexity of the problem, it was decided to use Computational Fluid Dynamics (CFD) code. CFD deals with the numerical analysis of the flow. According to the J. Mahaffy, 2014 the use of such an advanced tool is justified for the cases where 3D aspects play a key role. Furthermore, CFD codes continue to grow in significance for nuclear safety analyses despite modest guidelines for complex problem solving (Boyd, 2016).

Firstly, the numerical model of the NC was prepared. This enabled to model the detailed conditions in the reactor core. Using this model the wide spectrum of cases were analyzed. This allowed to determine operating safety limits for steady-state operation.

The capability of pool cooling system to cool down the converter was concluded from obtained characteristics.

The flow inside the NC was modelled with ANSYS tools. The flow domain (geometry) was prepared using SpaceClaim R17.2, then it was discretized using ANSYS Workbench Mesher 17.2 and the CFD simulation was run with ANSYS Fluent 17.2. The process of modelling to obtain preliminary results for steady-state took ca. 6 months where 60% of time took discretization of the domain. The calculation process was performed on the Świerk Computing Centre machine at the National Centre for Nuclear Research (NCBJ), which allowed to significantly reduce the time of calculation compared to the real-time needed for a single workstation. It is worth to mentioning that computational power needed to deal with one case took at least 3-4 hours of 400 CPUs. To prepare this thesis almost 70 test cases were run.

3.1 Domain

Modelled geometry is called domain. The region of interest consists of FP and coolant flow within the SbFP. Having considered the applicability of boundary conditions and their influence on the heat transfer within the SbFP the domain has to be broadened to the entire converter structure. The following paragraphs present subsequent steps of the analysis with several assumptions and simplifications.

Assumption

The heat is generated in the uranium core of the FP, which is coated with 0.7 mm aluminium layer on the sides. The conduction thermal resistance calculated from Equation 1.4 is 0.0004 K/W, while the convection resistance equals 0.0144 K/W (Equation

1.6).

Having taken into account negligible contribution of aluminium conduction resistance to total thermal resistance, it was assumed that aluminium layer does not reduce the heat transfer between uranium core and water. In addition, prospective maximum wall temperature without aluminium sleeve is anticipated to be greater than in real object as heat flux dissipation through aluminium takes place (1.5.3). As a result of the mentioned assumption, the heat transfer in aluminium layer was neglected and the heat flux from plate core was transferred directly to plate wall, which enables modelling only fluid volume.

Flow volume design

The flow volume is the geometry where the coolant is transported. The geometry was extracted from the CAD geometry with SpaceClaim. The converter CAD model was designed with Autodesk Inventor 2017, then it was exported to Standard for the Exchange of Product Model Data (STEP) and imported to SpaceClaim 17.2. Export to neutral file format may lead to some misrepresentations in the geometry. However, this issue is hardly possible to detect due to the complex geometry of the entire domain. Identified problems like overlapping geometries and gaps between volumes were corrected during flow volume extraction. No errors caused by misrepresentation were found within the cooling slots, which are the main region of interest. In Figure 3.1 the extracted flow domain is presented. Many small volumes which do not affect the cooling can be observed which is why some of them were deleted in agreement with the construction team.

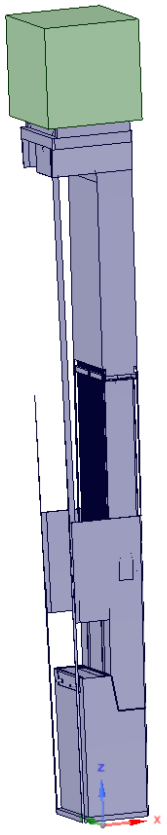

FIGURE 3.1: Preliminary flow volume.

For instance, the bypass between the aluminium sleeve and the curved block was neglected as the curved block shape can be fitted during manufacturing to the existing aluminium sleeve.

After several iterations of meshing, some simplifications were necessary to obtain a reasonable number of good quality elements. Consequently, the heat conduction by the sidewalls of the plate is not modelled because of the negligible size of the slot in this area. As it is presented in the Figure 3.2. The uranium fuel inside the plate is smaller than the cooling slot. In figure 3.3. section view through the

modelled FB is presented: blue, yellow and grey represents coolant flow, Fuel plates and side covers, respectively. Side covers are made from aluminium, so negligible energy generation is anticipated within their structures.

Another important modification in simulated geometry concerns filter. It was planned to be modelled integrally with the structure of the converter. Initial meshing trials showed that almost 2/3 of the elements were located in the filter. For this reason, it was modelled separately. In addition, the flow area by the filter is greater than the next section of the converter. Flow choking by the filter is negligible and has no important influence on the further coolant flow. As a result, the cross-section of the upper cover of the aluminium sleeve is considered as an inlet to the analyzed domain.

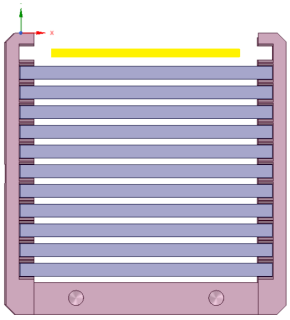

FIGURE 3.2: Section through the basket with plates. The aluminium coat hidden in the top plate to present uranium fuel inside plate.

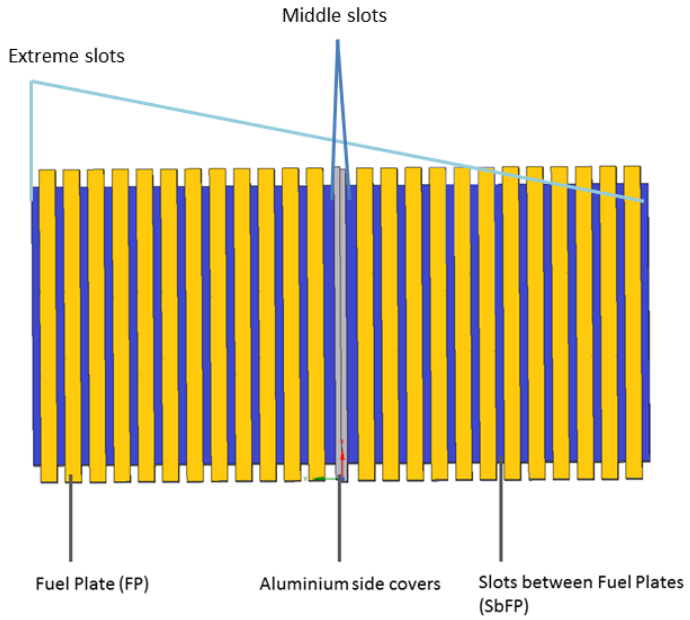

FIGURE 3.3: Cross section of FP, SbFP and side covers.

Converter coolant outlet

The outlet from the domain was defined in several options. The differences concerned either the independent cooling system or the use of reactor pool cooling system. Each option determined the outlet geometry and brought the need to compare and evaluate obtained results.

Initially, the autonomous cooling system was analyzed where the outflow was realized via orifice on the sidewall (marked in orange in the figure 3.4). The flow in such configuration was forced by the pump, which would have been placed on the side. To determine the cooling requirements, several cases were modelled with this geometry. The results are presented in the Chapter 4.

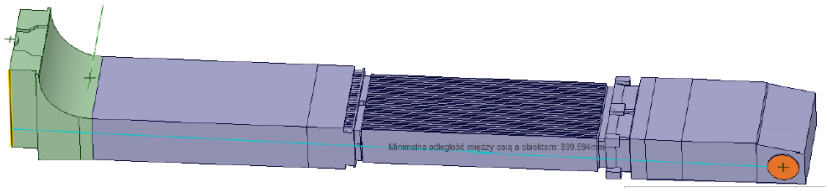

FIGURE 3.4: Flow domain for autonomous cooling system analysis.

Since the autonomous cooling system turned out to be hardly possible to design due to already existing installation in the reactor core and formal difficulties, the capability of the reactor pool cooling system to cool down the converter was studied. The use of the reactor pool cooling system brought many doubts on the converter outlet, which remained open question at that stage. The previous converter design was provided with four orifices located in the bottom plate of the block and a hole through the leg (Wierzchnicka, 2008). In current design, one of those is going to be applied. In the figure 3.5 the considered geometries for pool cooling option are presented (from the bottom: outlet via leg, outlet via bottom plate orifices and shorten domain).

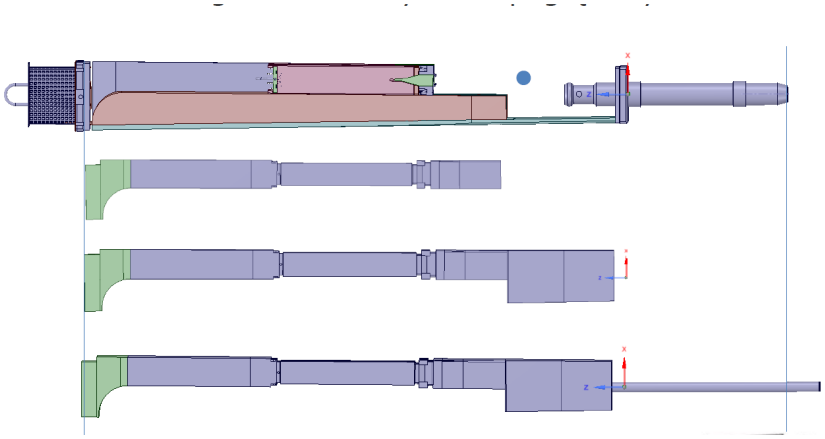

FIGURE 3.5: Considered domain sizes: outlet variations.

For all three geometries test cases were examined where following boundary conditions were applied:

- Case A: inlet velocity of 0.2m/s and outflow
- Case B: inlet velocity of 2 m/s and outflow

Boundary conditions for case A correspond to the reactor pool conditions, while the inlet condition for Case B assumes ten times higher coolant velocity. Since any observable differences in flow distribution occurred in Case A, the overestimated BC for Case B was defined in order to determine the impact of the flow contraction effect. In the figure 3.6 and 3.7 velocity and pressure along the one line chosen in the way to represent flow in the whole domain are presented. The line location is marked in red in fig. 3.6 in the top-left corner of the presented chart. Case B coolant velocity along the line for the test geometries is presented in the fig. 3.6. Red, green and blue line represent coolant velocity in a short domain, outlet via orifices and via leg, respectively. The lines match exactly until they exit SbFPs. In the fig. 3.7 pressure changes within analyzed test cases is shown. Any differences are observable on the chart, which means that modeled flow volume can be shortened, causing any uncertainties.

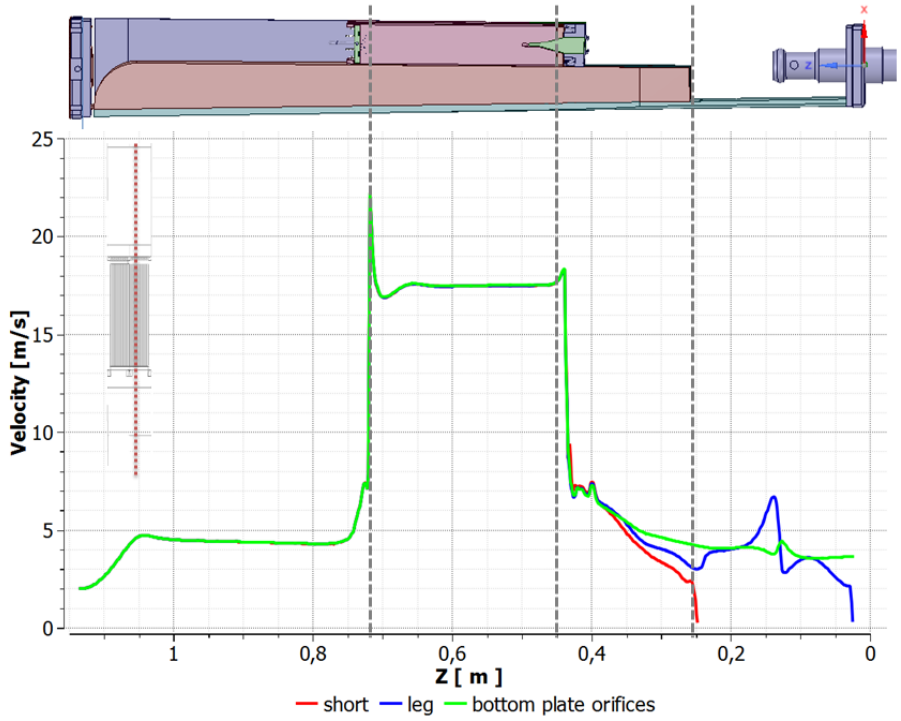

FIGURE 3.6: Velocities along red dashed line for case B.

Both velocity and pressure remain unchanged for all cases until the end of plates. Consequently, the differences caused by the variant geometries do not affect the flow in between plates and heat transfer in this area, so the modelled domain may be shortened as it is presented in the figure 3.8. As a result, the shortest geometry was chosen to model the heat transfer in pool cooling variant and remains a reference for presented in Chapter 4 for discussion of results.

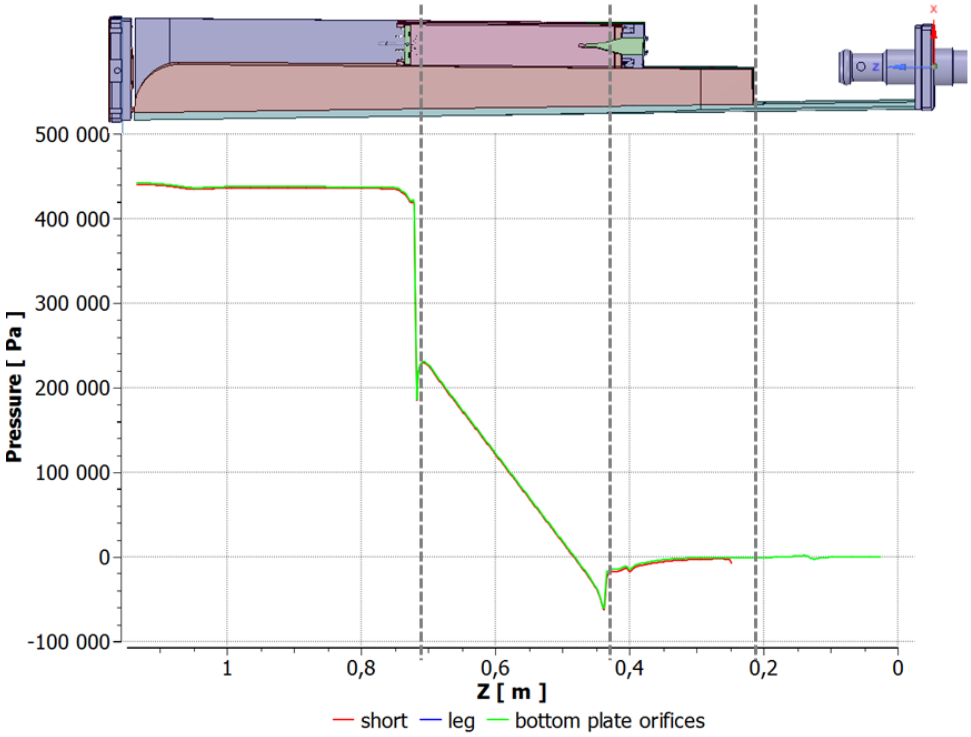

FIGURE 3.7: Pressures along yellow line for case B.

Flow volume dimensions

The final analyzed volume consists of 32 bodies which can be assigned to several zones: inlet, flow development zone, zone before the plate inlet, in between plates zone and outlet zone. (See Figure 3.8)

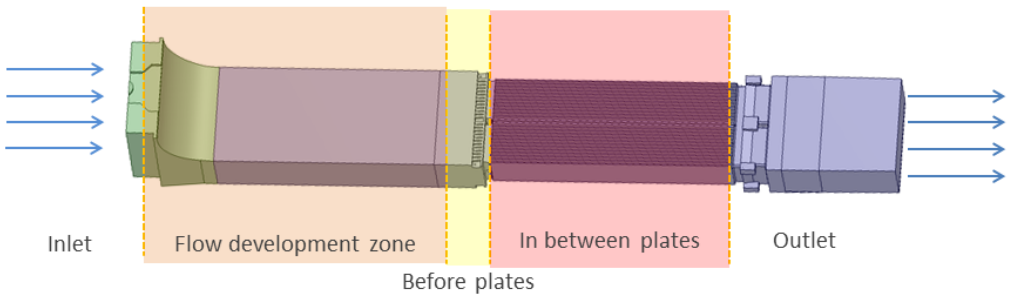

FIGURE 3.8: Flow domain characteristic sections.

General dimensions of the domain are as follows:

- Length of domain: 887 mm
- Inlet cross section: 13367 mm^2

- Outlet cross section: 7034 mm^2
- Slot width along x-axis: 48 mm
- Slot length: 280 mm

Three types of the SbFP were distinguished: two center slots between the cover and plate 22 regular slots between plates and two extreme ones whose parameters are presented in the Table 3.1. The slots are middle and extreme slots are marked on the Figure 3.3 while the other are the regular ones.

slot type	center	regular	extreme
width [mm]	1.90	1.40	1.30
hydraulic diameter [mm]	3.66	2.72	2.53
area [mm2]	91.20	67.20	62.40

TABLE 3.1: Slots dimensions.

3.2 Domain discretization

The mesh was generated with the use of ANSYS Mesher 17.2 Worksheet tool. The domain is split into 32 separate bodies, where 26 bodies stand for SbFP (See Figure 3.9). Domain complexity makes discretization of the problem challenging as the mesh resolution should cover both turbulence and heat transfer phenomena. According to G.Hansen, 2008 the CAD decomposition and discretization process are major bottlenecks in the modelling process. It is hardly possible to find specific guidelines due to the variety of requirements caused by the multi-physics nature of the simulation. This issue was also addressed during the converter model preparation.

The strategy for meshing was to optimize the number of cells in the bodies, so every area where possible the hexahedral cells were applied. This also has an impact on domain division. The general assumption is that the hexahedral cells are applied in regular bodies and others are filled with tetrahedral elements. The sequence of meshing was recorded with Mesher Worksheet 17.2 so that master and slave faces connections remained the same with following mesh generations and the mesh was consistent. The SbFP were meshed first with hexahedral cells. The size of the cell increases with the increasing distance from the slot inlet. Mesh in the SbFPs was defined as master to the neighbouring bodies that is why any change in slot mesh enforces neighbouring cells modifications.

The mesh orthogonal quality and skewness for reference mesh are depicted in the Figure 3.10 and 3.11. It can be observed that all of the hexahedral elements have orthogonal quality above 0.95 and skewness below 0.05, which indicates sufficient mesh quality accordingly to the ANSYS, 2016b. There are less than 1% tetrahedral

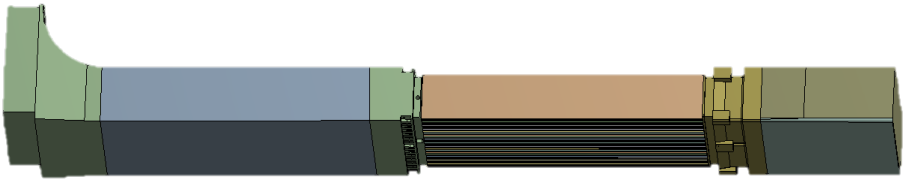

FIGURE 3.9: Domain division into 32 bodies.

parameter	definition
Bodies	32
Face zones	174
Nodes	16760446
Cells	21662091
Faces	58936748
Partitions	8

TABLE 3.2: General mesh information.

elements with skewness above required 0.95, which impact on final results is negligible. For fluid flow modeling the y^+ parameter is also defined. The wall y^+ [Equation 3.1] determines if *the influences in wall-adjacent cells are laminar or turbulent hence indicating the part of the turbulent boundary layer that it resolves* [M. Ariff, 2009b].

$$y^+ = \frac{u_\tau y}{v} \tag{3.1}$$

This measure makes it possible to divide near-wall region into three regions:

- $y^+ < 5$: viscous sublayer,
- $5 < y^+ < 30$: buffer region,
- $30 < y^+ < 300$: fully turbulent portion.

Moreover, some turbulence models define requirements for y^+, so it is essential to control this value for mesh during turbulence modeling.

In the Figure 3.12 the wall y^+ on the slot walls and inlets is presented. The highest values can be observed for the neighboring middle slot walls and it is noticed that maximum is about 30, which is a margin value for buffer region. The detailed analysis showed that the wall y^+ obtains the highest values at the inlet of the slot and the value decreases with the distance to the slot inlet. The average the wall y^+ value at the slot wall ranges between 7-12, the wider the slot the higher the wall y^+. On the narrow walls of extreme and middle slots a significant y^+ reduction can be observed.

As it was noticed by T. Jinyuan, 2006, it takes significant time and effort to obtain successful mesh despite variety guidelines and indications arising from turbulence model selection. The discretization of the converter model preliminary took more than a month so as to achieve the first converged solution. It is also important to

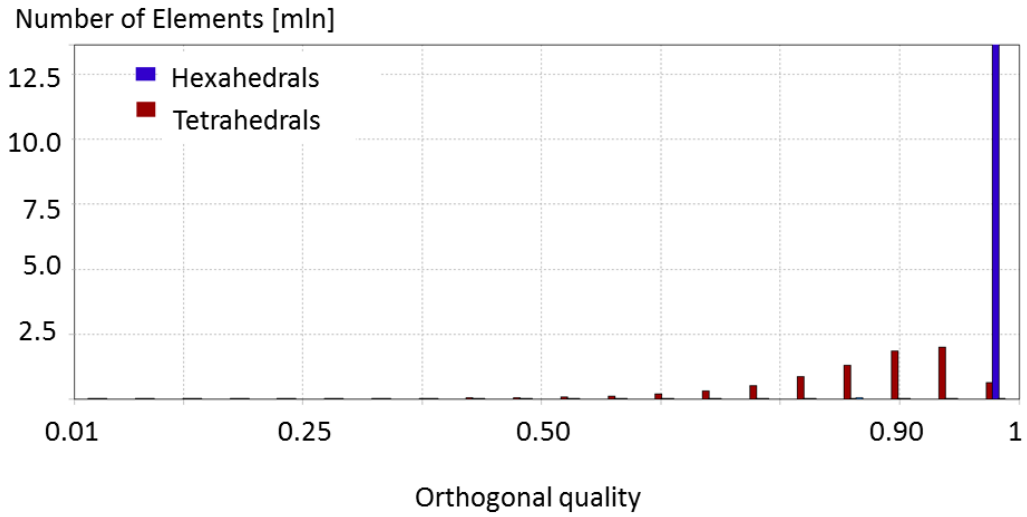

FIGURE 3.10: Orthogonal quality of the reference mesh.

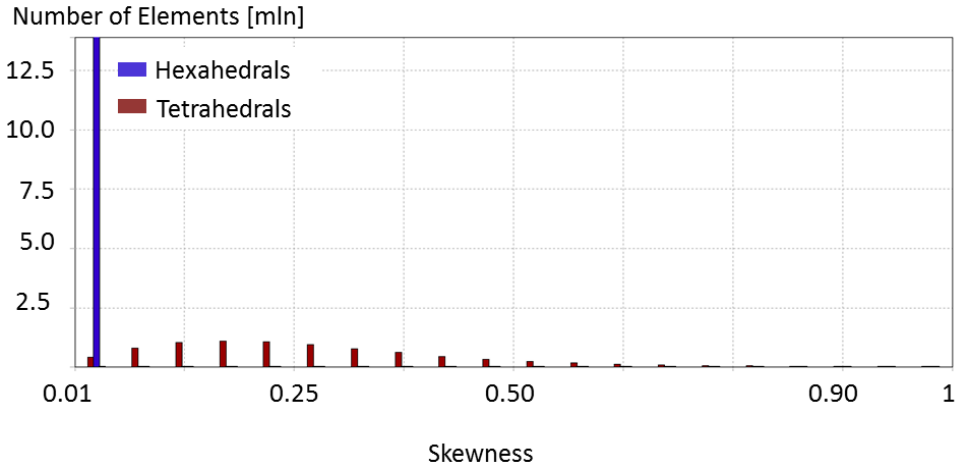

FIGURE 3.11: Reference mesh skewness.

notice that the discretization is performed on local workstation, so the time depends on computer components, mainly CPU and RAM memory.

According to ANSYS Fluent Theory Guide [ANSYS, 2016a] the recommended number of cells to cover boundary layer equals 10. It is stated above that the reference mesh does not fulfill this requirement. Although the mesh is really coarse for boundary layer modeling, it is claimed to be the reference one since proper wall treatment was applied to the model. Details on the wall treatment are described in section 3.3.3 (Turbulence model).

Several difficulties with grid convergence were met thus it was decided to redefine the mesh for consecutive analyses, which are not described in that thesis. The domain primarily will be shortened to the SbFPs and the plenums above and below them, owning to the modifications in sets design. The mesh for the forthcoming transient analyses such as loss of coolant flow and natural convection for air cooling is prepared in compliance with ANSYS Fluent User Guide.

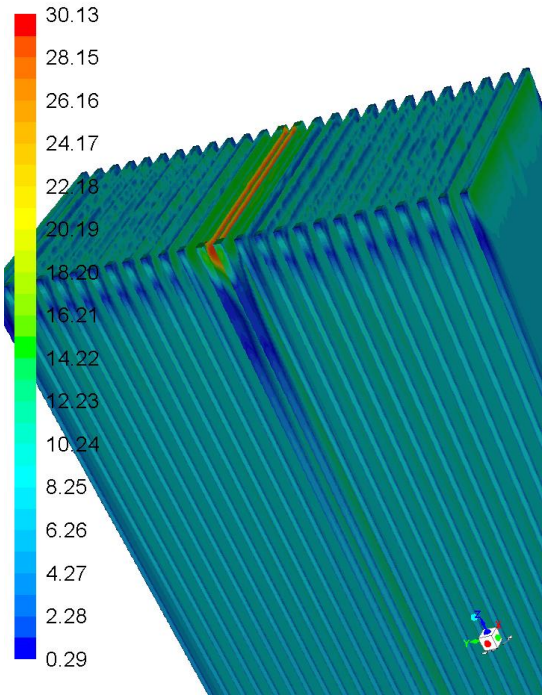

FIGURE 3.12: y^+ depicted on the slot walls and inlets.

3.3 Numerical Setup

The converter model was prepared and run with ANSYS Fluent 17.2 This is a 3D simulation where full geometry is modelled. No symmetry conditions were applied due to very specific orientation of the model. The calculations are time-independent, only steady state results will be analyzed. The solver is pressure based type with SIMPLE pressure-velocity coupling. Standard differencing scheme was chosen for pressure, while momentum, turbulence and energy are treated with the second order upwind scheme. The calculations were performed with convergence criteria equal to 0.000001 for all residuals. Under relaxation factors for pressure, momentum and energy were 0.35, 0.4 and 0.9 respectively. The compressibility effect can be observed with temperature changes, while pressure impact on physical parameters of the fluid are neglected. Above mentioned settings were applied to all the cases unless it is stated clearly in case of the specific description. Numerical model settings summary is presented in Table 3.3.

Option	Definition
Solver type	Pressure-Based
Velocity formulation	Absolute
Time	Steady
Model	Energy: On
	Viscous model: Realizable k-ϵ
	Near-wall Treatment: Enhanced wall functions
Pressure -Velocity Coupling	Scheme SIMPLE
Spatial discretization	Gradient: Green-Gauss Based
	Pressure: Standard
	Momentum: Second Order Upwind
	Turbulent Kinetic Energy: Second Order Upwind
	Turbulent Dissipation Rate: Second Order Upwind
	Energy: Second Order Upwind

TABLE 3.3: Numerical model settings.

3.3.1 Working fluid

The working fluid is water. Firstly, incompressible fluid was considered but for heat transfer calculation, the changes of the fluid properties with temperature were taken into account and applied to the model as it is presented in Table 3.4. No phase change is anticipated, so the model was run as a single phase.

fluid temperature	density	specific heat	thermal conductivity	viscosity
[K]	[kg/m3]	[J/kg K]	[W/m K]	[Pa/s]
323	988.1	4027	0.64	0.000548
333	983.3	3977	0.65	0.000467
343	977.9	3926	0.66	0.000404
353	971.9	3973	0,67	0.000355
363	965.4	3821	0.67	0.000315
373	958.8	3769	0.68	0.000282
383	951.1	3717	0.68	0.000255

TABLE 3.4: Working fluid parameters applied to model.

3.3.2 Initial and boundary conditions

The first calculation were obtained for the following initial conditions: 323 K flow inlet temperature and 174 kPa operating pressure, which corresponds the sum of atmospheric pressure and the 7m water column. The boundary conditions were applied as 8.83 kPa pressure difference, which is an equivalent of water column in the analyzed geometry. The following conditions represent the pessimistic conditions where cooling water in MRR pool cooling circuit work with its upper limit of 323 K (50 °C) and the flow is driven only by the water potential energy.

For required pump power determination the initial pressure difference of 8.83 kPa was reduced by factor 2 with following test cases in order to determine minimum value for sufficient cooling conditions. As a result the test cases for 4.4 kPa,

2.0 kPa and 1.75 kPa were run. Maximum temperatures obtained for the test cases for 1.75 and 2.0 kPa overstep the ONBR limit, thus the pressure difference of 2.3 kPa was applied to meet the minimum ONBR value. For pool cooling system variant also higher values of pressure difference were considered, in particular 1.4 m H_2O water column, which is the minimum for MRR pool cooling system. The spectrum of analyzed test cases is presented in the Figure 3.13.

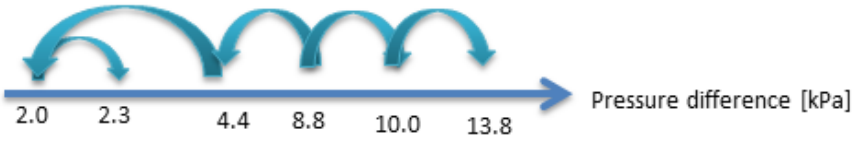

FIGURE 3.13: Applied pressure difference determination.

The heat transport is modeled in the second part of this study. The averaged values were applied for preliminary calculations and then a profile of heat flux on the slot wall was prepared. The heat flux values were delivered by the neutronic team as a result of Monte Carlo simulation of neutron transport within the MARIA Reactor. Further details are presented in Heat Flux subsection 3.3.4.

Condition	Definition
Inlet	pressure-inlet Gauge Total Pressure 0 Pa Initial Gauge Pressure 0 Pa temperature 323K
Outlet	pressure-outlet Gauge Pressure -8.829 kPa
Walls	material: aluminium density: 2719kg/m^3 specific heat 871 J/kgK thermal conductivity 202.4 $W/(m*K)$ stationary wall; no slip condition thermal conditions: heat flux profile (Details in Subsection 2.3.4)
Fluid Zone	water-liquid (Details in Subsection 2.3.1
Operating Conditions	pressure: 174.09 kPa operating temperature 323K

TABLE 3.5: Initial and Boundary conditions.

The gravity influence was taken into account. Initially, the gravity vector was applied on z axis direction with value: $-9.81 m/s^2$ neglecting the tilt from vertical (See Figure 3.14). In the next step, this issue was corrected and the tilt impact on flow distribution was investigated. The Results are presented in Chapter 4 in subsection 4.1.1. Summary of initial and boundary conditions is stated in Table 3.5.

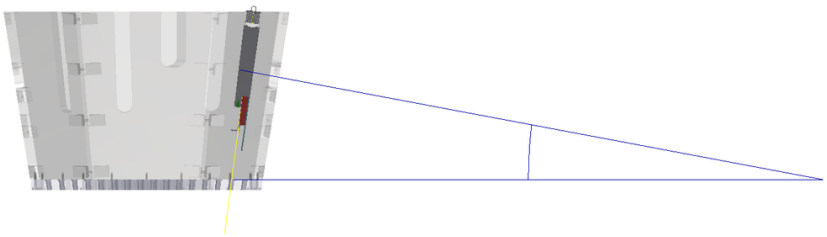

FIGURE 3.14: Converter block tilt.

3.3.3 Turbulence model

Due to the complex geometry with flow obstacles (split into millimeter-size slots and rejoin for the outlet) the need for turbulence modeling occurred. In addition, M. Abdollahzadeh, 2017 implies that flow between vertical plates is frequently a traditional one, which amplifies proper turbulence modelling.

Having considered the domain size and complexity, RANS approach has been applied. Reynolds-averaged Navier-Stokes (RANS) is the most economic choice for computing complex flows [ANSYS, 2016a]. It models both large and small eddies taking time-average of variables [J.E. Jaramillo, 2007]]. Those models introduce turbulent viscosity and solve two additional transport equations to compute Reynold stresses. The most common RANS models are $k-\epsilon$ [B.E.Launder, 1974] and $k-\omega$ [Wilcox, 1988].

Initially, it was hardly possible to predict, which turbulence model would be the most suitable. There are general guidelines for turbulence modeling in nuclear industry but none favor any turbulence model.

Furthermore, reliable boundary conditions forced the size of the domain so multiple aspects had to be taken into account. The advantages of k-ϵ models seemed to be the most suitable for development zone. In contrast to the superior performance near wall of k-ω model was intuitive choice for cooling slots modelling [(J. Mahaffy, 2014)].

After the convergence of the solution for turbulence and heat transfer simulation with one turbulence model, here it was SST $k-\omega$, was obtained the following models were tested: Standard $k-\epsilon$, RNG $k-\epsilon$, Realizable $k-\epsilon$ with enhanced wall function.

The choice of tested models is based on the ones used by A. Gandhir, 2011 and A.S. Alzwayi, 2013 for fuel bundle modelling and heated vertical channel flow simulation respectively.

The heat transfer conditions applied for turbulence model choice were simplified to uniform heat flux on the walls, which corresponds to the average heat generated in the neutron converter. The SST $k-\omega$ model was chosen for the first case runs since it covers advantages of $k-\omega$ near wall and $k-\epsilon$ for bulk fluid as in is stated

in Mentner, 1994. Furthermore, the experience of the CFD team in NCBJ and evaluation presented by C.C. Liu, 2012 shows that this RANS model produces promising results for cases where improved wall treatment plays significant role . However, the SST $k-\omega$ is recommended one, some doubts regarding the conservativeness of the results occurred. That is why to obtain the most conservative value of ONBR, the Realizable $k-\epsilon$ with Enhanced wall functions was chosen for further simulations due to the highest wall temperature obtained with this turbulence model. According to C.D. Argyropoulos, 2014 Realizable $k-\epsilon$ model satisfies *realizability constraints on the normal Reynolds stresses and the Schwartz inequity for turbulent shear stresses* resulting in improved performance for channel flow modelling. Moreover, Realizable $k-\epsilon$ model was used for nuclear safety analyses in studies lead by Z.Chen, 2015.

The criteria of turbulence model choice was the highest wall temperature obtained for simplified heat load boundary conditions in order to model worst possible condition in steady state performance. Although SST $k-\omega$ produced the greatest value of all as it is presented in the Figure 3.15, it was taken as a numerical error because this value significantly departs from the other obtained for this slot. The numerical error might be a result of insufficient grid density as in Mentner, 1994 is mentioned that this model gives satisfactory results with the first gridpoint as far out as $y^+ = 3$. It can be observed that Realizable $k-\epsilon$ model overestimates values in middle slots, obtaining the highest values for the regular slot comparing to the other models. In addition, the coolant velocity profile at the slot inlet, in the middle of the plate height and at the slot outlet were compared. The detailed comparison of the profiles showed that the Realizable $k-\epsilon$ model produces the lowest values of velocity magnitude at the heated zones. Having considered the velocity impact on heat transfer coefficient the greatest wall temperatures are anticipated thus the analysis is conservative (takes into account the worst possible scenario).

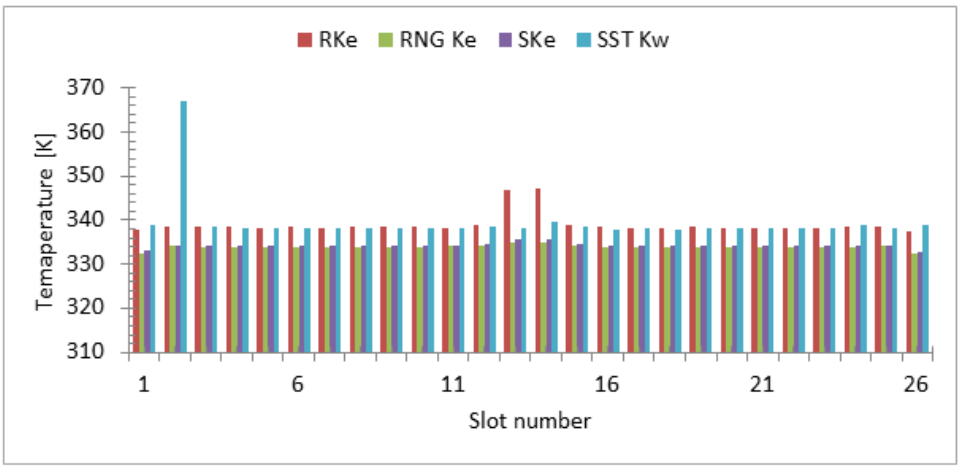

FIGURE 3.15: Maximum wall temperature with respect to the slot and turbulence model.

Realizable $k-\epsilon$ model overview

Governing Equations:

Transport equations for k and ϵ are presented with Equations 3.2 and 3.3.

$$\frac{\partial}{\partial t}(\rho k)+\frac{\partial}{\partial x_j}(\rho K u_j)=\frac{\partial}{\partial x_j}[(\mu+\frac{\mu_t}{\sigma_k})]+G_k+G_b-\rho\epsilon-Y_M+S_k \tag{3.2}$$

$$\frac{\partial}{\partial t}(\rho\epsilon)+\frac{\partial}{\partial x_j}(\rho\epsilon u_j)=\frac{\partial}{\partial x_j}[(\mu+\frac{\mu_t}{\sigma_\epsilon})]+\rho C_1 S\epsilon-\rho C_2\frac{\epsilon^2}{k+\sqrt[2]{\nu\epsilon}}+C_{1\epsilon}\frac{\epsilon}{k}C_{3\epsilon}G_b+S_\epsilon \tag{3.3}$$

where

$$C_1=max[0.43,\frac{\eta}{\eta+5}],\eta=S\frac{k}{\epsilon},S=\sqrt[2]{2S_{ij}S_{ij}} \tag{3.4}$$

- G_k stands for the generation of turbulence kinetic energy due to mean velocity gradients,
- G_b represents generation of turbulence kinetic energy due to buoyancy,
- Y_M is the contribution of fluctuating dilatation in compressible turbulence to the overall dissipation rate,
- C_2 and $C_{1\epsilon}$ are constants,
- σ_k and σ_ϵ are turbulent Prandtl numbers,
- S_k, S_ϵ are user-defined source terms.

The k equation is the same as for Standard k-ϵ and RNG k-ϵ models, while the ϵ equation does not involve the k production in the second term on the right-hand side and G_k term is not involved as in the other k-ϵ models.

3.3.4 Heat flux

The fission rate within the plates is non-uniform because the thermal neutrons from the reactor core meet first the plate, which is the nearest to the core center. Consequently, the heat generation takes the same pattern: the closer reactor core the more energy is produced. The wall heat flux data obtained from Monte Carlo simulation was applied to CFD model as heat flux profile on the slot wall. The heat flux data was delivered for the steady state conditions (Courtesy of G. Madejowski). The data are assumed to be credible, so any uncertainties caused by the heat profile were investigated.

The average power generated by each plate is presented in Figure 3.16, the plate numeration rises with red arrow presented in the Figure 1.11. The 25^{th} plate is the one closest to the reactor core center and the most loaded one. Plate number 13 represents two aluminium covers of the baskets where hardly any power is generated. Since the aluminium covers of the sets do not stop neutrons, more particles reach 12^{th} and 14^{th} plate that is why local maximum of fission rate and generated power

can be observed. The more fissions take place the more heat is generated so that in 1^{st} plate local peak occurs as a result of increased reflected neutron flux in this position.

Figure 3.17 represents the heat flux profile applied on slot wall in Fluent. In particular it is 25^{th} plate, however similar trends are observable on every plate. The higher values occur at the right edge, which is located closer to the reactor core center. The maximum value is located at the bottom of the hottest edge. The maximum heat flux equals 201.94 kW/m^2 for the MRR operating with its maximum power (30 MW_{th}). The flux field is divided into 160 rectangular regions in that such discretization was used for neutron transport modelling with MCNP code by neutronic team.

Simplified heat load conditions were applied to determine region of safe operation for the converter. The uniform heat flux was equal to: 42.85 kW/m^2, 82.59 kW/m^2, 177.43 kW/m^2, which corresponds respectively to average heat flux for all plates, average heat flux for most loaded plate, maximum local heat flux, which occurred for entire converter. The values presented in this paragraph correspond with MRR operating at 24 MW_{th}, which is the highest operating power in recent years.

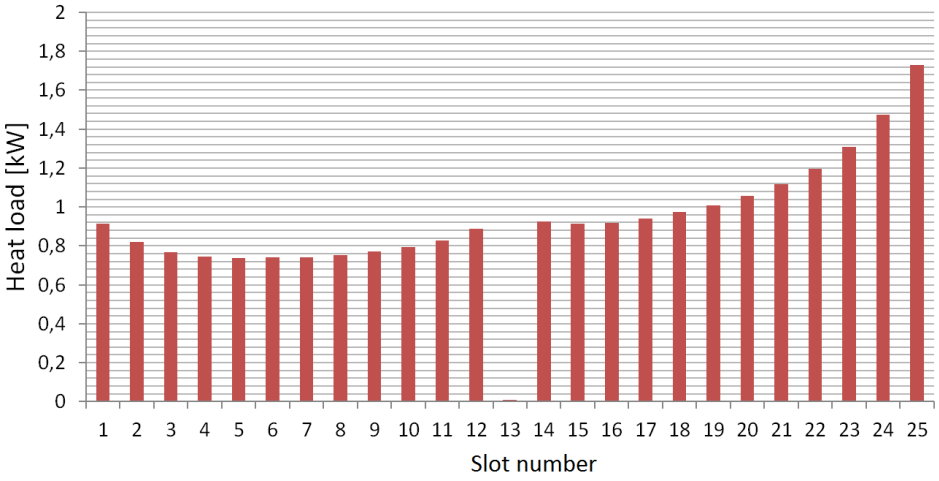

FIGURE 3.16: Power generated in each plate.

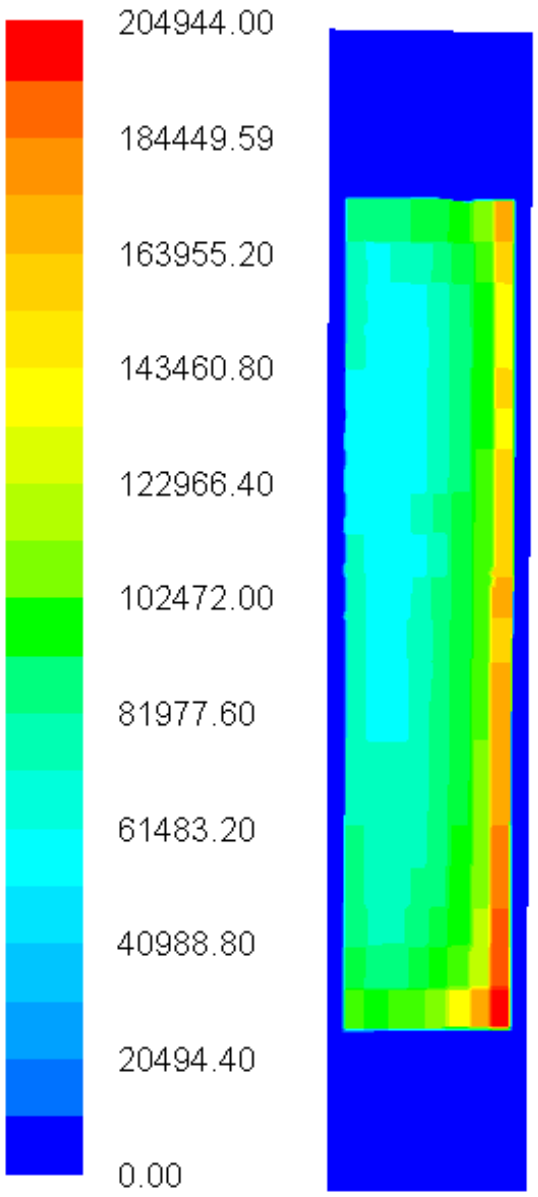

FIGURE 3.17: Heat flux contour (W/m^2).

4 Calculation results analysis

4.1 Flow distribution

In this section the coolant distribution within the domain is presented. The influence of block inclination and possibility of domain reduction are discussed in the subsequent paragraphs. Presented results are obtained for pressure difference equal to 8.829 kPa and realistic heat load condition applied on the slot walls (heat flux profile on Figure 3.17). The pressure difference applied to the model was based on the information found on documents and reports on MARIA research reactor, in 2020 the measurement in the four location of reactor core shown that this value ranges from 8.800 to 9.235 kPa. The mentioned measurements were performed on the cylindrical structures, the additional test on the converter mock-up both on out-of-core stand and in-core measurements are planned before applying for consent for exploitation of the neutron converter.

For the discussion of the results the following definitions have to be stated: Coolant velocity in Fluent is also called velocity magnitude, here also called as velocity; U-velocity is the velocity vector component along x-axis; V-velocity is the velocity vector component along y-axis; W-velocity is the velocity vector component along z-axis.

4.1.1 Inclination impact on flow distribution

The IV-B socket at MRR is inclined by almost 9 degrees from the vertical direction (See Figure 3.14) thus some impact on the flow distribution both among the SbFPs and within one slot were anticipated.

In the Figure 4.1 the coolant distribution among SbFPs is depicted, hardly any difference can be observed as the values differ at the sixth digit. Although, summary mass flow in the SbFP remains unaffected by the fact of block inclination, the flow distribution within the domain may be affected so the velocity profiles were studied.

Figures 4.3, 4.4 and 4.5 represents coolant velocity at the back, the center and the front of the slots inlets respectively (Figure 4.2), the profiles are sampled from the lines parallel to the narrowest plate and slot walls. Converter front is understood as a position in which the curved aluminum block is behind the sets with plates, slot back is the location close to the curved aluminum block but slightly shifted to front to picture the behavior of bulk fluid not boundary layer. It can be observed that the profiles almost perfectly match. The same situation is met while plotting velocity

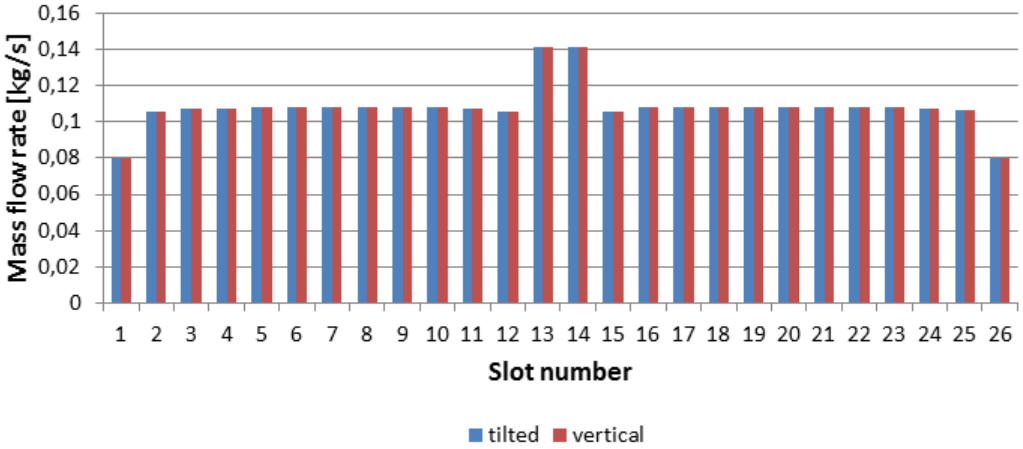

FIGURE 4.1: Coolant mass flow distribution.

components, so it legitimizes lack of gravity influence on the flow distribution in y-direction.

Figure 4.6 presents the velocity within one regular slot, here the profiles with and without inclination also match, similar profile was generated for the other slots at different slots heights and all of the samples perfectly agree. Summing up, the flow distribution within the domain is unaffected by the block inclination however it has to be considered that the pool cooling is driven by the suction pumps. As a result, the water is forced to flow form the top of the pool to its bottom during steady state operation and a forced convection mechanism is a dominant one. Although, it does not indicate the same for loss of flow accident for future transient scenario modelling where the flow is driven by free convection.

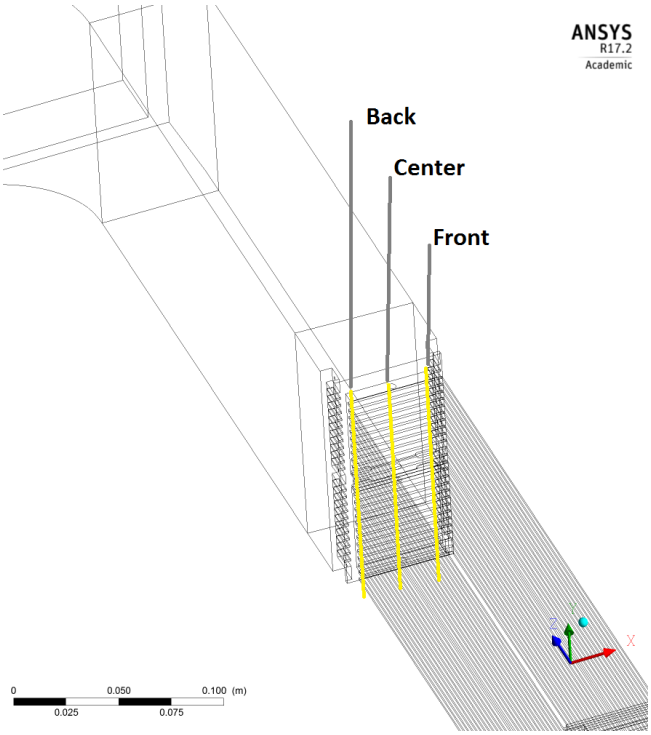

FIGURE 4.2: Sampling lines location at the inlet to the SbFP.

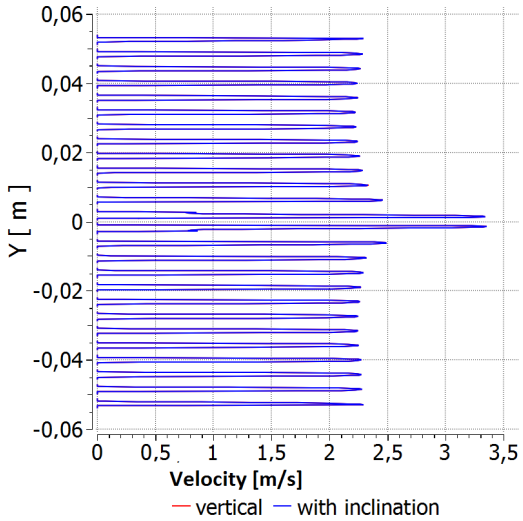

FIGURE 4.3: Coolant velocity at slots inlets - at the back of the plates.

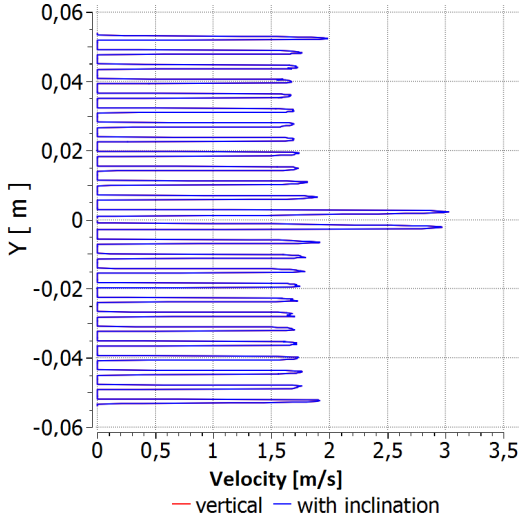

FIGURE 4.4: Coolant velocity at slots inlets - at the SbFPs center.

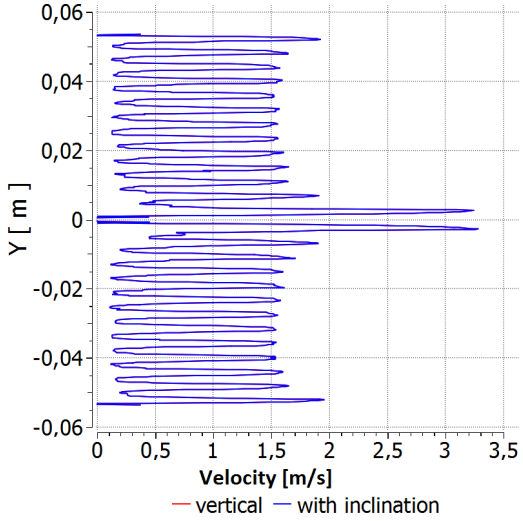

FIGURE 4.5: Coolant velocity at slots inlets - at the front of the converter.

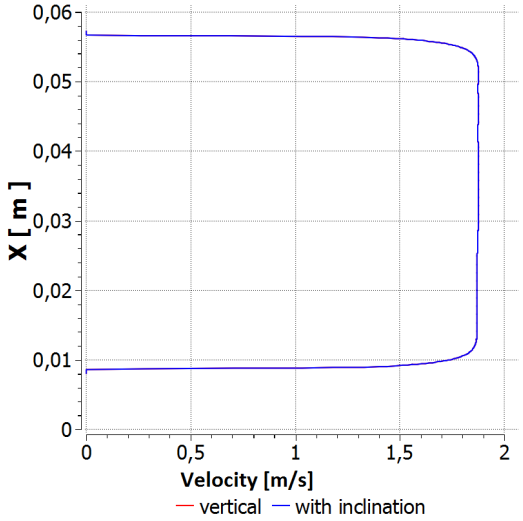

FIGURE 4.6: Coolant velocity across the slot (along x-axis).

4.1.2 Domain reduction

Figures 4.7 - 4.12 represent velocity profiles at three locations: at the SbFPs inlets, in the middle of the SbFPs height and the SbFPs outlets for the reference and reduced domain. The reference domain is the one which is presented in Chapter 3 in the Figure 3.8. The reduced one contains 26 separated SbFPs only. The boundary conditions for the reduced domain were applied as:

- velocity components profile at the SbFPs inlets and outflow,
- velocity magnitude profile at SbFPs inlets and outflow,
- velocity magnitude profile at both inlets and outflows,
- velocity components profile at inlets and outlets,
- pressure profile at inlets and outlets.

Next the reduced domain calculations were run for 5000 iterations and the velocity profiles were compared with reference domain. For the BC applied as velocity profiles the solution residuals stopped at 10^{-2} with visible oscillations, which is a sign of problem with solution convergence. Moreover, the comparison of the velocity profiles gave unsatisfactory results. The promising results were obtained for pressure profiles BCs. Neither any problems with solution convergence nor significant changes in velocity profile shape were observed. The velocity profiles comparison for the pressure BCs are presented in Figures 4.7 - 4.12. Coolant velocity profile shape at the SbFPs inlets for reduced domain is in good agreement with the reference one. Although the difference in value for extreme and regular SbFPs occurs, the greatest difference is observed for the regular SbFPs and equals about 0.2 m/s (ca. 15%) [Fig. 4.7]. For the middle ones both the value and profile shape are in good agreement with reference case.

The U-Velocity profile [Fig. 4.8] for reduced domain at the SbFPs inlets correspond to reference for eight SbFPs, others remain underestimated. For the 5^{th} and the 8^{th} SbFP the u-velocity component seems to be completely different than the reference one. The shape of the v-velocity profile [Fig. 4.9] for the reduced domain agree with the reference one, however the values remain slightly higher for the reference domain. Such behavior indicates that the solution at the boundaries is affected by the applied BCs, which is a source of possible uncertainties. W-velocity profile [Fig. 4.10] shape at the inlet for reduced domain corresponds to the reference one, the effect of flow area contraction is conserved in the profile at that location however, the values are overestimated about 0.1 m/s (ca. 5%) each.

Figures 4.11 and 4.12 present coolant velocity at the middle height of SbFP and at the outlet of the slots. Significant differences between velocity profiles for reference and reduced domain are observed: the values for reduced domain are overestimated for external and regular SbFPs, while the values for in middle SbFPs are about 0.3

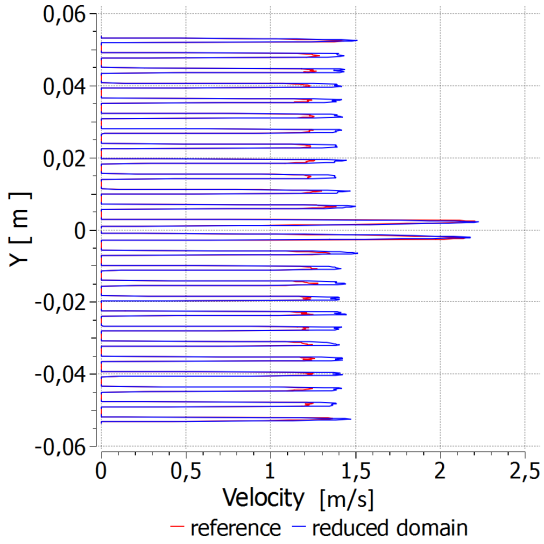

FIGURE 4.7: Velocity at SbFPs inlets.

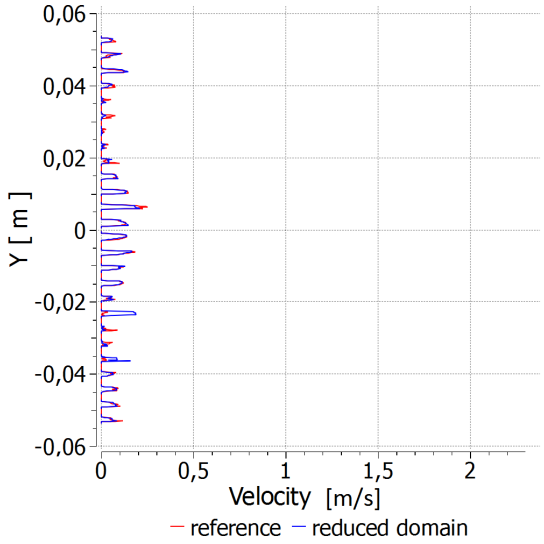

FIGURE 4.8: U-Velocity at SbFPs inlets.

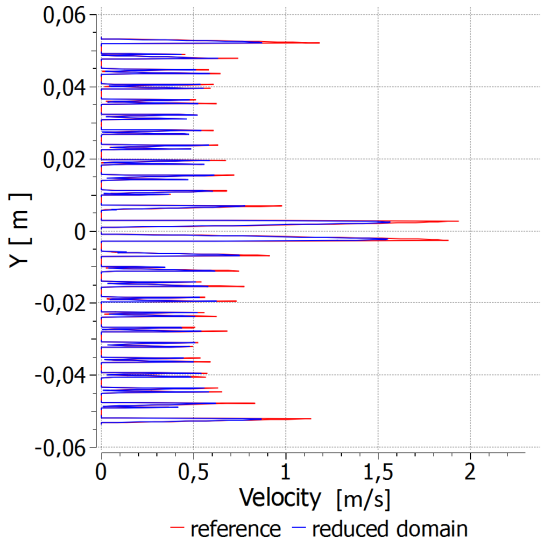

FIGURE 4.9: V-Velocity at SbFPs inlets.

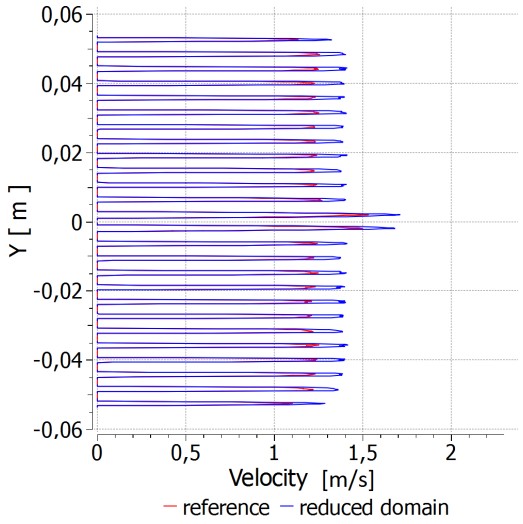

FIGURE 4.10: W-Velocity at SbFPs inlets.

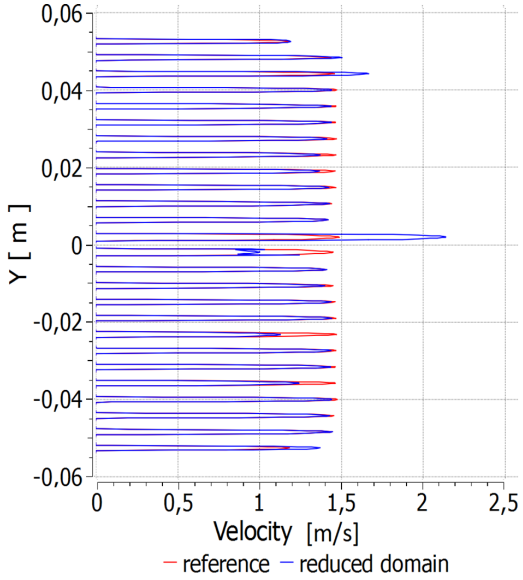

FIGURE 4.11: Velocity at middle height of SbFPs.

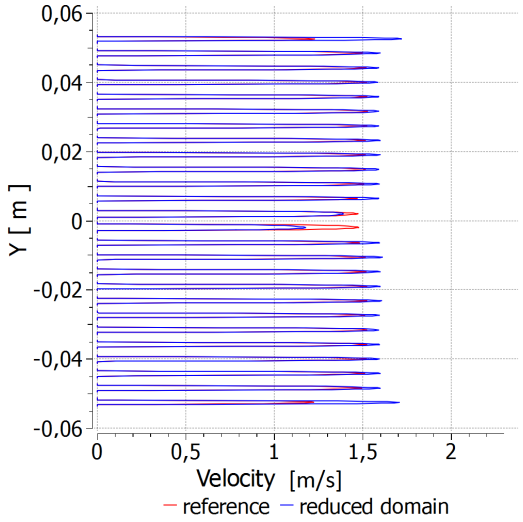

FIGURE 4.12: Velocity at SbFPs outlets.

m/s (ca. 20%) lower than in the reference case. Moreover, the shape of the reference w-velocity profile for each set corresponds to the theoretical velocity profile for the pipe: the closer to the set wall the smaller velocity is. This behavior does not occur for reduced domain where the maximum velocities are observed in the extreme SbFPs, which are also the narrowest ones. The overestimated value of velocity magnitude and w-velocity for reduced domain are alerting as it may lead to underestimation of peak cladding temperature. Furthermore, the velocity components in x- and y- directions were underestimated, which indicated reduced eddies impact at the SbFPs inlets. Since the nuclear safety analyses are conservative ones, it was decided to use reference domain in order to avoid uncertainties induced by domain reduction.

4.1.3 Vortices's at the SbFPs inlets

In the Figure 4.13 the velocity along two line is presented. The straight lines was chosen so the represent velocity changes within the whole domain. It can be observed that the lines superimpose except for the plates area as a result of specific line locations in this area: blue line represents the velocity at the slot center while red one near slot wall. The velocity increases from the domain inlet, reaches peak at the slot inlet and another local peak at the slot outlet. Small peaks appear slightly before slot inlet as the set holder and the spring induce flow speed up in their neighborhood. Similar behavior occur at the bottom of the set with directive bars. The significant reduction of flow area cross section from square duct to set of milliliter size SBFPs causes speed up of the coolant velocity within the SbFP. Such contraction impose eddies production at the SbFPs inlets as it was mentioned in section 1.5.5. Figure 4.13 shows velocity along z-direction at the center of each slot (Series number in legend corresponds with the slot number). Three slot types according to its width can be acknowledged. Dashed blue and purple lines (Series 13 and 14) rocket up to almost $3m/s$, then slope within next 2 mm and velocity stabilizes at $2m/s$ 2 cm from the slot inlet. Continuous red line and dash-dot blue line correspond to extreme SbFPs (1^{st} and 26^{th}), the curves reach maximum and goes down up t $1.6m/s$. Other lines represent regular SbFPs, the peak at the inlet is $0.4m/s$ higher than the velocity reached after stabilization of the flow within the slot which equals $1.9m/s$.

The active plate zones begin at $0.68m$, the flow in the SbFP is expected to be developed in that region in order to prove this hypothesis the velocity vectors are presented in the Figure 4.15. Vectors are plotted on the cross section filled with temperature contours, the contour map at the bottom of the picture shows heat flux applied on the slot wall. The velocity profile at the beginning of heated zone is the mean laminar velocity profile for the slot though in the middle SbFPs the maximum velocity is slightly shifted to the non-heated wall. Moreover, the contraction effect is boosted in the middle and extreme SbFPs as the frame, which protect plates from replacement in vertical direction, make the flow enter those SbFPs at certain angle.

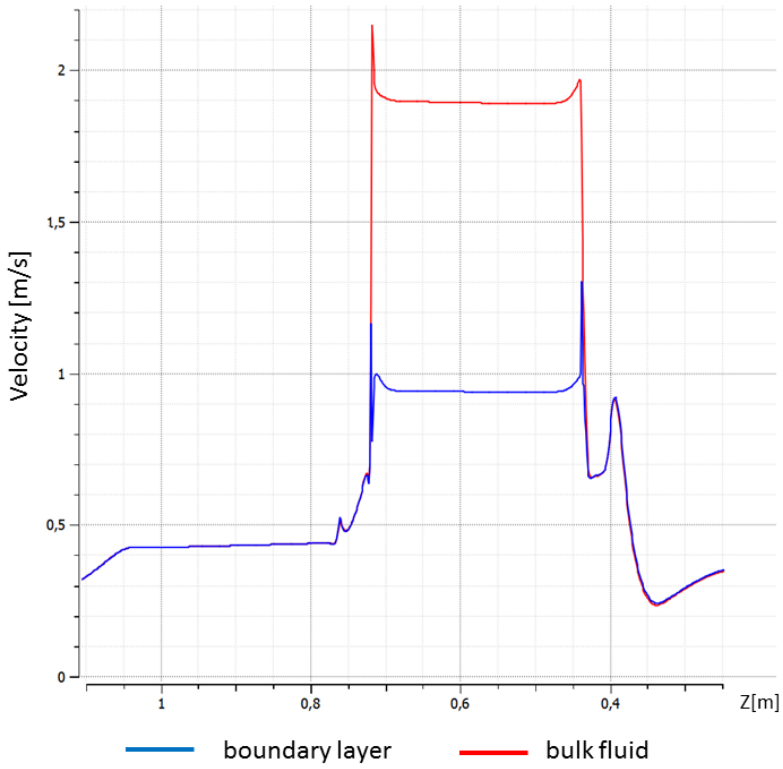

FIGURE 4.13: Velocity of the coolant along straight line in z-direction.

This inclination angle of slot entrance for middle slots is depicted both on Figure 4.14 and 4.17.

In the Figure 4.16 the w-velocity is depicted, w-velocity component is the one parallel to z-axis, along main flow direction in this case. The values are in general lower than one in this case due to opposite turns of flow direction and CAD model orientation. Positive values location indicate existence of eddies especially at the inlet to middle and extreme slots, for regular slot the eddies are hardly visible.

Since SbFPs has rectangular cross-section and the edges dimensions vary significantly depending on the point of view. On this plane the frame which keeps FPs in place impacts the flow, acting as the backward facing step for the flow. As a consequence, the eddies on the narrow wall of SbFPs are different from the ones observed in previous paragraph. Figures 4.17 - 4.19 show velocity vectors viewed from the longer slot edge side for middle, regular and extreme slot. The flow contraction effect is visible on all three figures as the velocity vectors as they do not reach the slot wall at the slot entrance. In the figure 4.17 velocity vectors in the middle slot are presented. The effect of the flow inclination is observable as the first row of vector is tilted to the back. At the point where active plate zone start the flow attached to channel wall so eddies do not affect heat transfer in this region. It is worth to notice that the flow is not fully developed at the beginning of active zone in order to determine the place where the coolant flow is fully developed the velocity profile where sampled. Figure 4.20 shows coolant velocity profile at five locations in the middle slot. The samples where taken at the inlet to the slot (orange line), 2 cm far from the

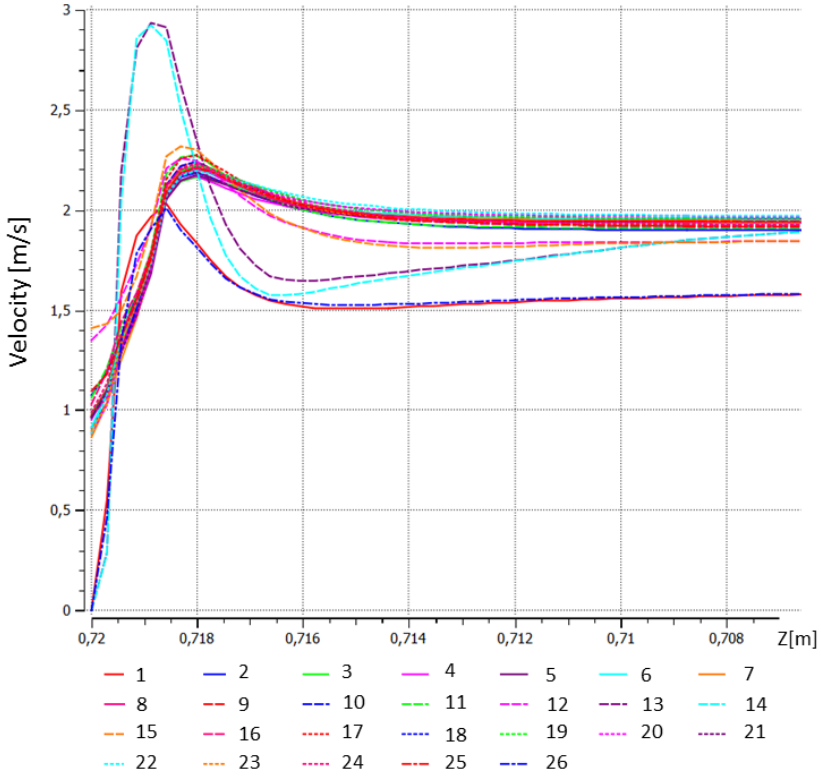

FIGURE 4.14: Velocity at the center of cooling SbFPs.

inlet (dark blue line), 4 cm from inlet (green line) etc. The flow is fully developed 20 cm far from the inlet where the turbulent velocity profile is observed.

In addition the eddies are longer comparing to the one analyzed above. In the middle slot the inlet velocity is the greatest one.

Figure 4.18 shows coolant velocity vectors in regular slot. The flow re-attach to the wall much closer to the slot inlet than in the middle slot. The vectors at the inlet are tilted slightly in y-direction due to holding wire and a handle existence. The coolant have to flow over the obstacles and enter channel at certain angle. Figure 4.21 show that the flow develops closer to the channel inlet than in the middle channel because 6 cm from the inlet the turbulent flow velocity profile is observable.

Coolant velocity vectors in extreme slot are presented in figure 4.19. At the point where active zone start the flow in attached to the slot wall. In the vectors row closer to the slot the flow is not truly reattached as the velocity vectors are not parallel to the wall. The flow in the extreme SbFP is fully developed 12 cm far from the slot entrance, which is faster than in the middle channel.

Having considered size of generated eddies and location of active zone, it is concluded that the eddies impact on heat transfer conditions is negligible. Comparing the flow development in each slot type, it can be observed that the inclination angle of flow entrance and channel width are key parameters which impact flow development within a slot.

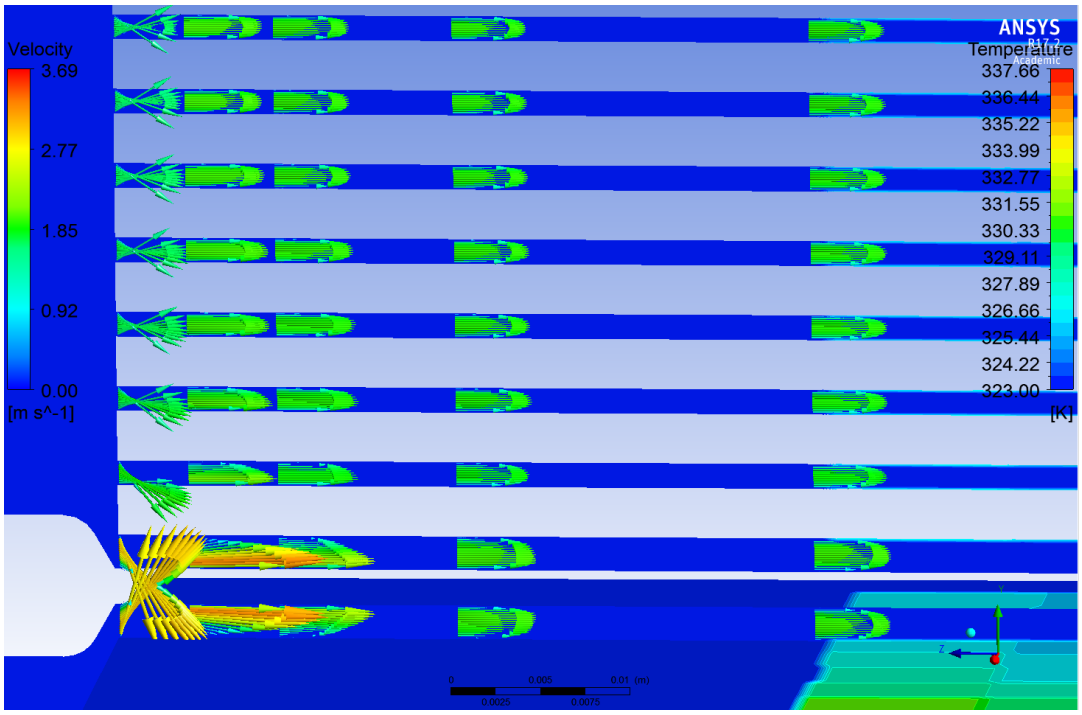

FIGURE 4.15: Velocity vectors at the SbFP inlets.

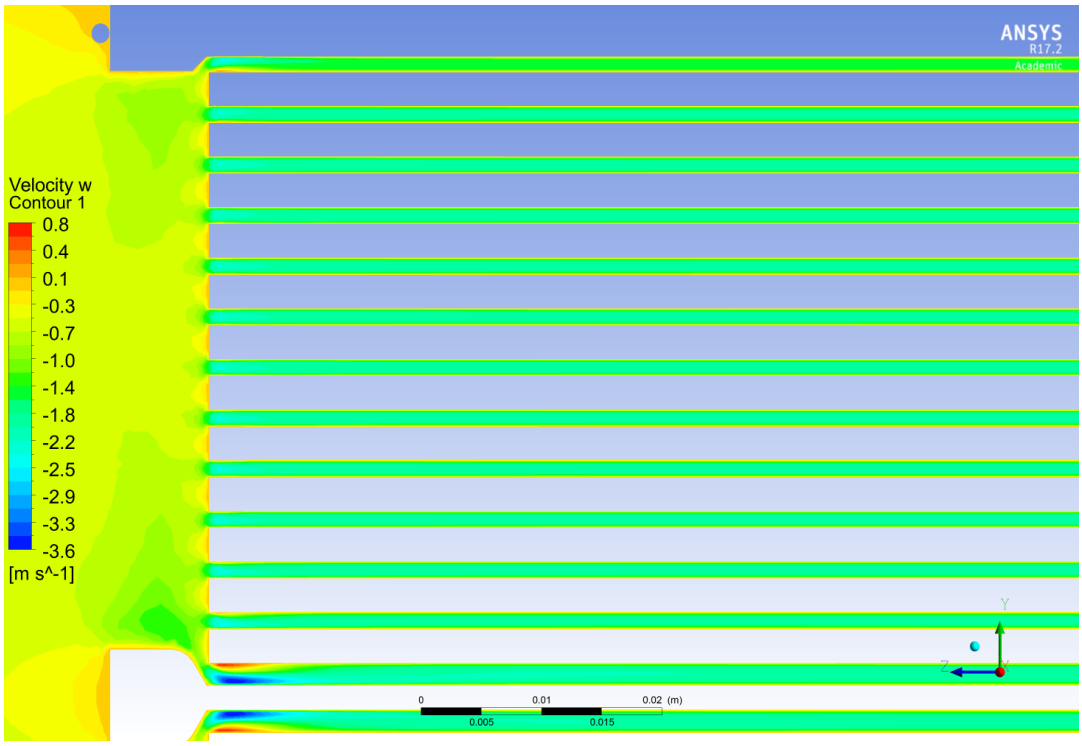

FIGURE 4.16: Velocity along flow direction at SbFP inlets. (Negative values are caused by opposite turns of flow and CAD model axis.)

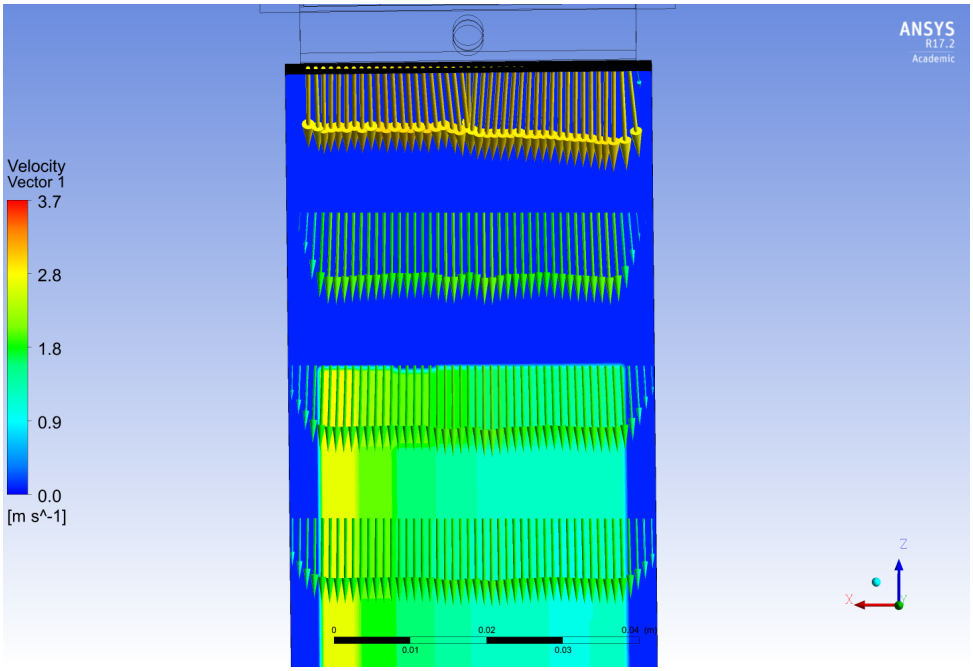

FIGURE 4.17: Velocity vectors at the center of middle SbFP - view from the side.

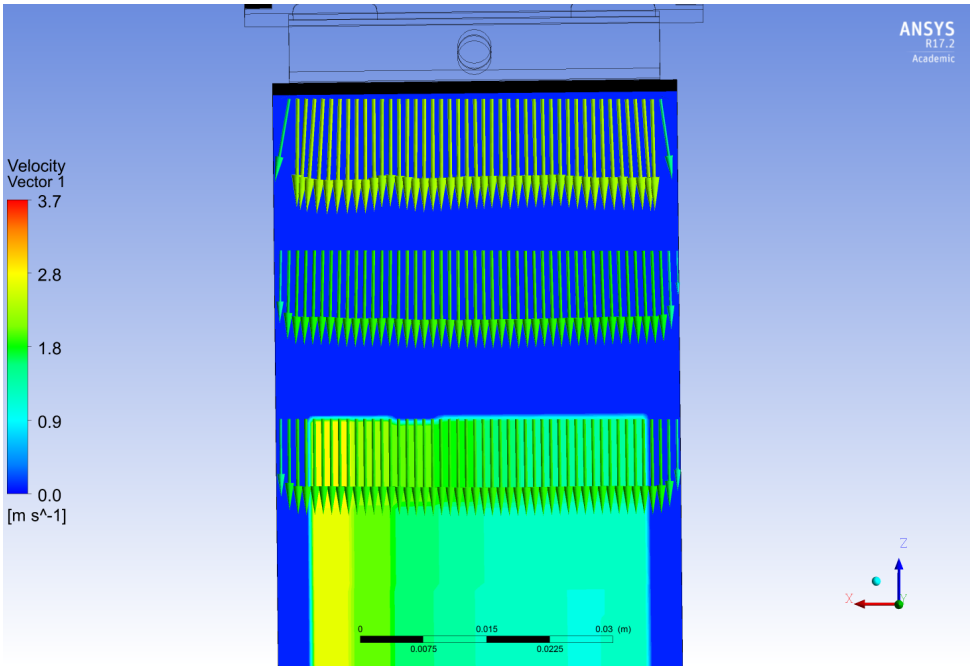

FIGURE 4.18: Velocity vectors at the center of one regular SbFP - view from the side.

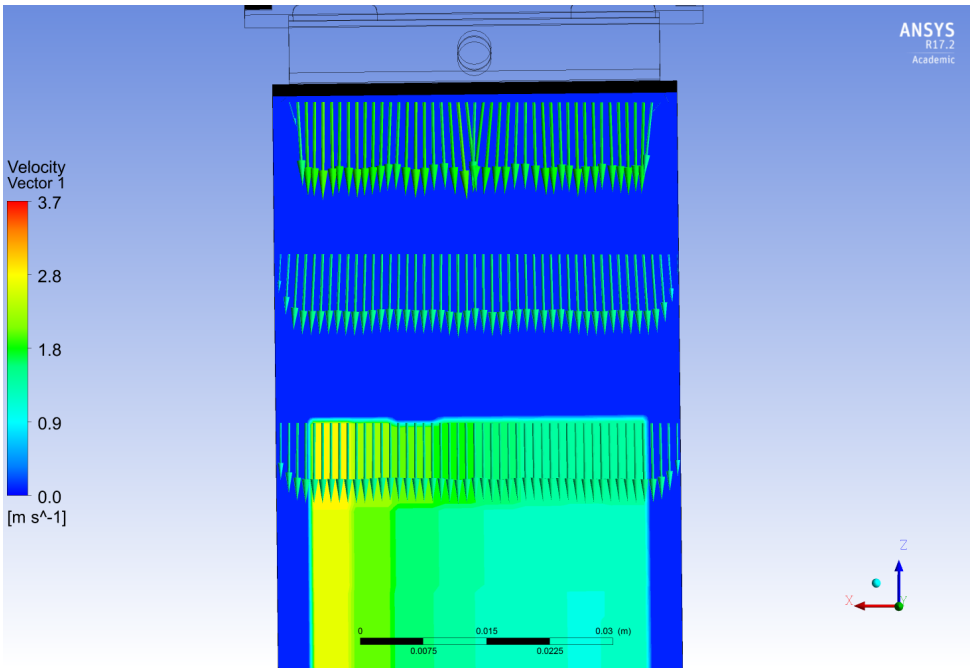

FIGURE 4.19: Velocity vectors at the center of the extreme SbFP - view from the side.

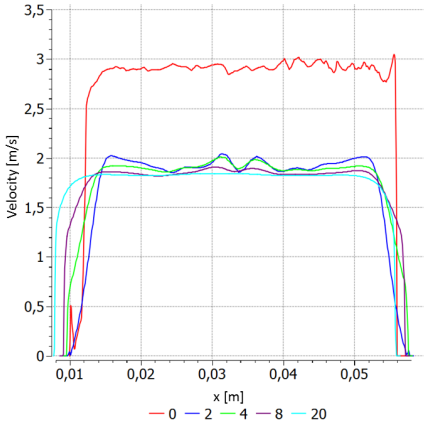

FIGURE 4.20: Velocity vectors at the center of middle SbFP - view from the side.

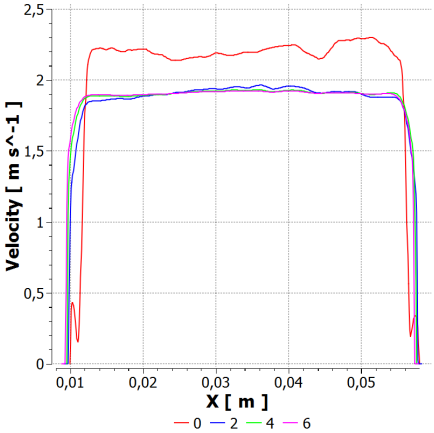

FIGURE 4.21: Velocity vectors at the center of one regular SbFP - view from the side.

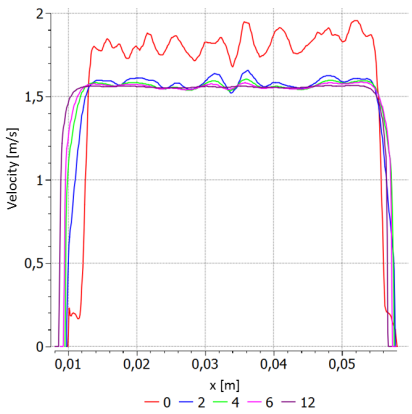

FIGURE 4.22: Velocity vectors at the center of the extreme SbFP - view from the side..

4.2 Heat flux field for IVB socket in MARIA

Figure 4.23 presents heat taken up from the plates, the 25^{th} SbFP received maximum energy on the grounds that both side walls consist of FP which are located nearest reactor core. The 26^{th} SbFP adjoins only one FP, thus exchanges moiety energy than 25^{th} SbFP. Similar phenomenon occurs on the opposite site of the converter symmetrically to the 26^{th} slot. Although the peaks are smaller, the relative difference in exchanged heat is comparable. The 13^{th} and 14^{th} SbFP adjoins aluminum side covers that is why local minimums are observed in those SbFPs. Local peaks in 12^{th} and 15^{th} SbFPs corresponds to the ones at 12^{th} and 14^{th} FPs presented in the Figure 3.16 since the more neutrons enter those plates due to the gap comprising of aluminum covers.

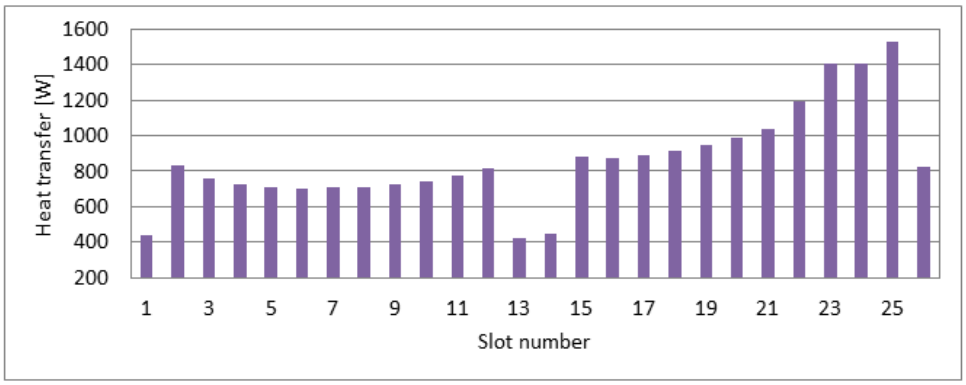

FIGURE 4.23: Heat exchanged by each slot.

In the figure 4.24 coolant mass flow rate for each slot is presented. Thus the flow is forced by the pressure difference and nonidentical slot size, flow distribution among SbFPs is nonuniform. The greatest mass flow is observed in the middle (13^{th} and 14^{th}) SbFPs which have the biggest cross section, while the smallest coolant flow rate occur for the extreme SbFPs, which are the smallest ones. Mass flow in other SbFPs remains at the same level, however tiny differences can be observed. Having considered only regular SbFP the velocity profile for each set can be compared to a laminar velocity profile encountered in pipes and ducts. Described features appear independently from the pressure difference.

Coolant heat up in each slot is shown in the Figure 4.25, the shape of the columns is in good agreement with the one presenting exchanged energy. With the decrease of the pressure difference the temperature difference increases as the less coolant mass flow exchanges heat with the plates. The global maximum occurs for the 25^{th} SbFP and three local maximums are observed for the 15^{th}, 12^{th} and 2^{nd} SbFP. The maximum temperature difference equals to 10 K for the 25^{th} SbFP at 1 kPa pressure difference. Also four minimums appear at the 1^{st}, the 13^{th}, the 14^{th} and the 26^{th} SbFPs regardless pressure difference. The smallest coolant heat up appears at 10 kPa for both the 25^{th} and the 25^{th} SbFP equals 0.6 K.

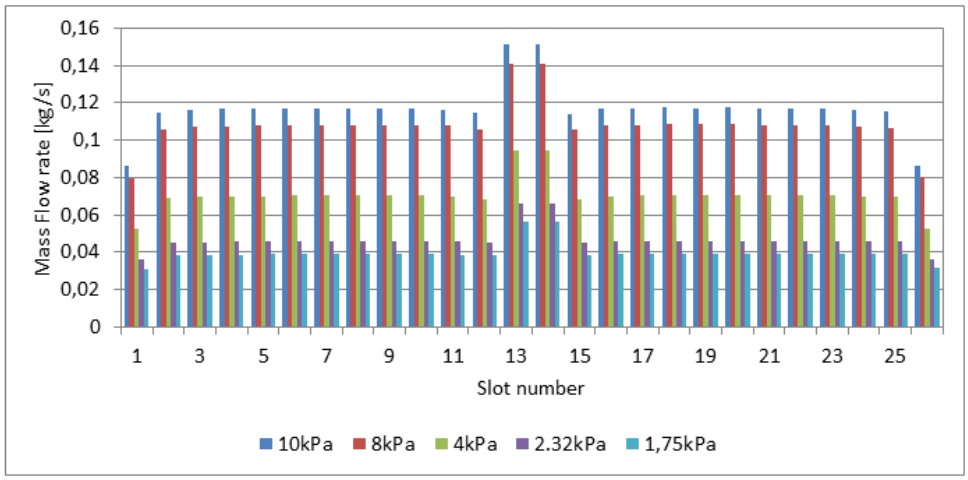

FIGURE 4.24: Coolant mass flow rate in the SbFPs with regard to pressure difference and slots numbering.

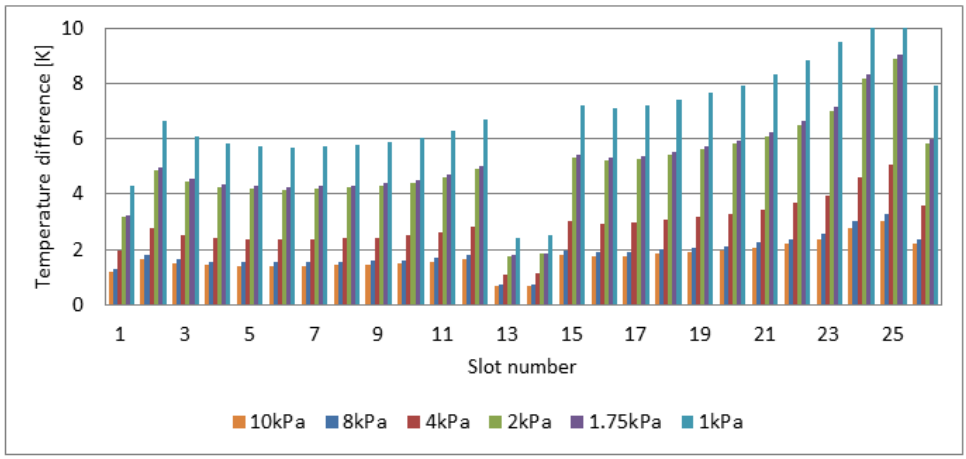

FIGURE 4.25: Temperature difference between SbFP outlet and SbFP inlet.

Peak cladding temperature (PCT) with respect to pressure difference is shown in the Figure 4.26. Reduction of the pressure difference causes general increase in the maximum wall temperature occurring in each slot. In addition, up to 2.32 kPa the PCT appears in 26^{th} SbFP, with further pressure difference decrease the PCT shows up in 25^{th}. Note that saturation temperature at 174 kPa equals to 382K, the results for 1 kPa and 1.75 kPa overcome this temperature so probably boiling occurs and applied model is not further suitable for such BCs. For 2 kPa pressure difference the shift of PCT occurrence may be induced either by increased cooling requirements for this slot or by numerical error as the PCT equals to 381.7 K. Having considered that the minimum operable pressure difference for MRR equals to 13.7 kPa, the values below 8 kPa pressure difference for analyzed domain are hardly possible to occur thus for given heat load conditions the pool cooling is sufficient to fulfill heat removal requirements for the neutron converter. As a result, autonomous cooling system do not have to be designed to cool down the installation at steady state operation.

Wall temperature contour map is presented in the Figure **??**, it can be observed

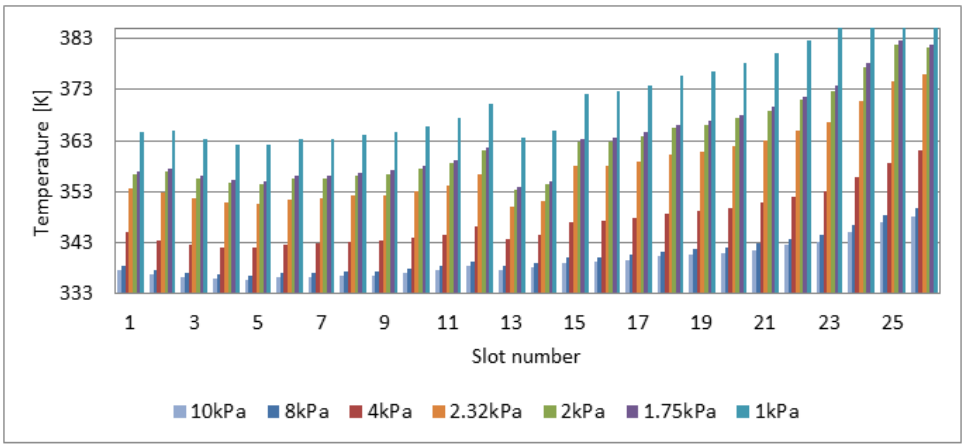

FIGURE 4.26: Maximum wall temperature with regard to pressure difference and slot number.

that the temperature contours are in good agreement with the heat flux contours shown in Figure 3.17 in Section 3.3.4. The characteristic shifts in temperature contour shape are caused by heat exchange from fluid to wall side in the hottest regions.

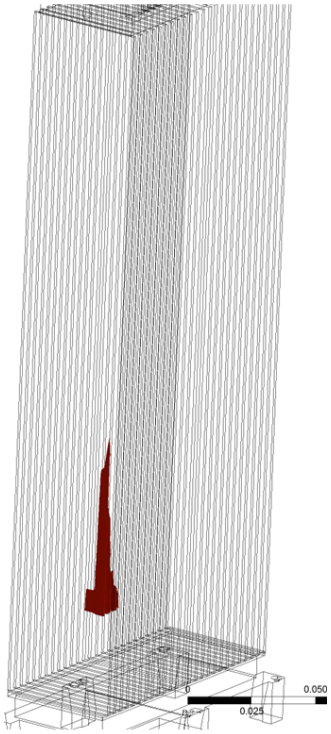

FIGURE 4.27: Isosurface of peak cladding temperature.

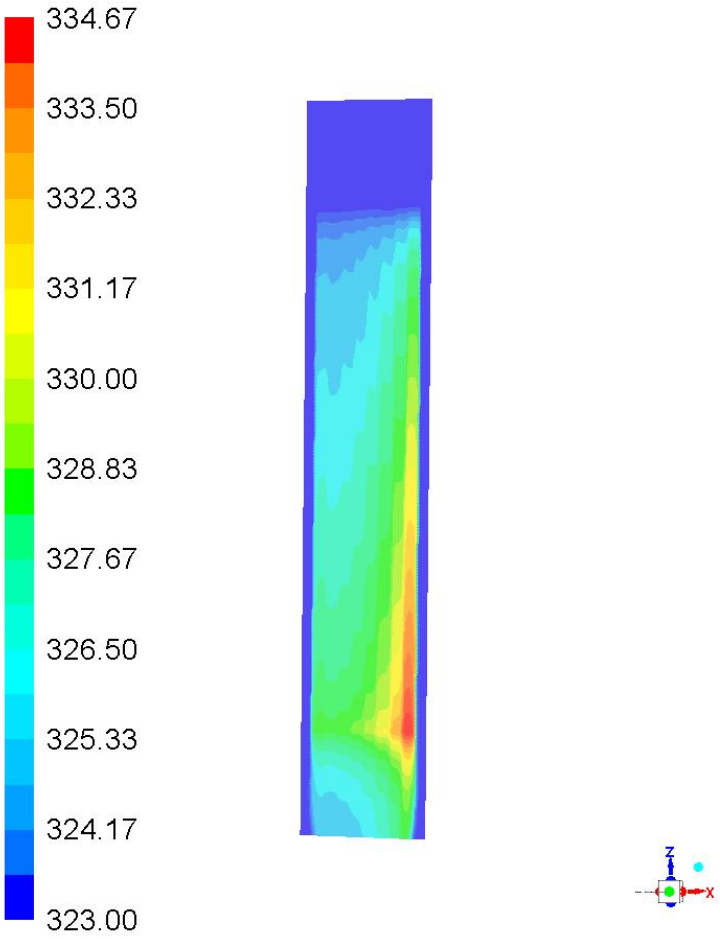

FIGURE 4.28: Coolant temperature closest to the wall (FP).

Figure 4.28 shows the coolant temperature of the coolant boundary layer of the plate with the greatest volumetric heat source (the one located closest to the reactor core) with coolant flow coresponding to 13.7 kPA pressure difference, which is a nominal value for normal exploitation of MARIA Research Reactor pool cooling system. The maximum temperature observable on the neurtron converter core equals to 350 K, 335 K for coolant which fulfil the safety limit for the reactor experiments, which stands for non boiling during normal operation.

5 Conclusions

The presented work studies the main thermal-hydraulic aspects that allow to determine the limits for sufficient heat removal conditions for Neutron Converter which is a unique component for BNCT test facility, by means of computational fluid dynamics analysis of steady state thermal hydraulic performance of installation.

First of all, the hydraulic conditions of the installation were determined keeping the reactor pool cooling conditions in mind. Secondly, the simplified heat load conditions were applied to determine the heat removal requirements by means of boundary pressure difference reduction to obtain the minimum coolant flow rate needed to ensure safe operation in steady state. Then, the realistic heat flux field was applied on the slots surfaces and the influence of the pressure difference was analyzed. Finally, the capability of the MRR pool cooling system to cool down the neutron converter was studied. Both maximum wall temperature and the temperature difference between inlet and outlet to the heated zone were analyzed as a main thermal-hydraulic parameters. The conclusions of the performed studies are presented in the following paragraphs.

Item	Value	Unit
Generated Power		kW
Coolant Inlet Temperature	323	K
Coolant Outlet Temperature (for the most loaded slot)		K
Coolant Outlet Temperature (for the entire installation)		K
Coolant Outlet Temperature (for the most loaded slot)		K
Average Temperature Difference (for the entire installation)		K
Maximum System Pressure		kPa
Minimum System Pressure		kPa
Total Coolant Flow Rate		kg/s
Coolant flow rate		
- in extreme slot		kg/s
- in regular slot		kg/s
- in middle slot		kg/s
ONBR		

TABLE 5.1: Preliminary thermal-hydraulic characterization.

In terms of further developments of the thermal-hydraulic assessment of the installation it is planned to:

- narrow the CFD model to the most loaded slot in order to resolve and evaluate both the hydraulic and the thermal boundary layers;

- validate the obtained result with another CFD code (either OpenFOAM or QuickerSim toolbox for Matlab are considered);
- determine cooling conditions in the air as it is planned to change the arrangement of the fuel plates;
- investigate transient conditions such as loss of coolant accidents or power peak.

A Grid sensitivity study

In order to determine whether the solution is independent from the grid four mesh variants in the region of interest were prepared. The channel mesh was controlled by predefined number of hexahedral elements created on the edge, the comparison of the plate meshes is presented in the Table A.1.

mesh variant	V3	REF	V1	V2
number of elements				
streamwise	437	500	562	625
wall-normal	9	10	11	12
spanwise	84	96	108	120
total number of elements per plate	269192	400000	566496	775000
total number of mesh elements in whole domain	18547797	21662091	27641004	33865306

TABLE A.1: Slots discretization details.

The reference case setup was run with those meshes and the results were compared. The parameters which were compared are average coolant velocity, coolant heat up in every SbFP and a maximum wall temperature in each slot. Then the relative error between reference mesh and each variant was calculated (Equation A.1).

$$E_r = \frac{a_{ref} - a_{v_{1,2,3}}}{a_{ref}} \tag{A.1}$$

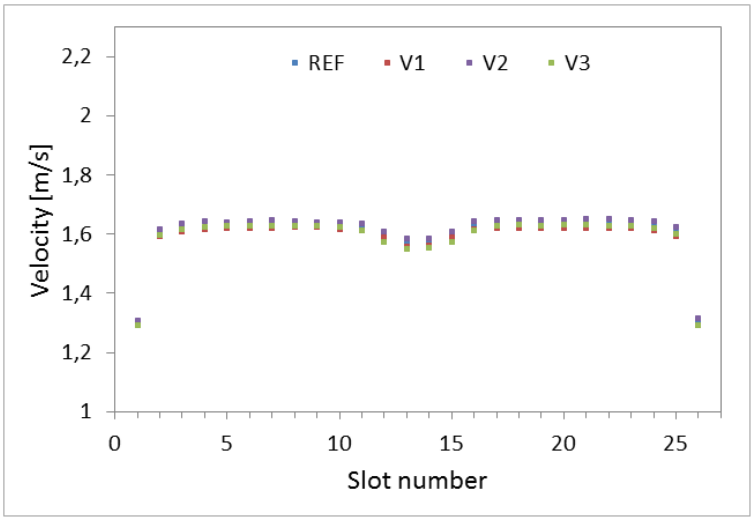

FIGURE A.1: Volume averaged coolant velocity in SbFP.

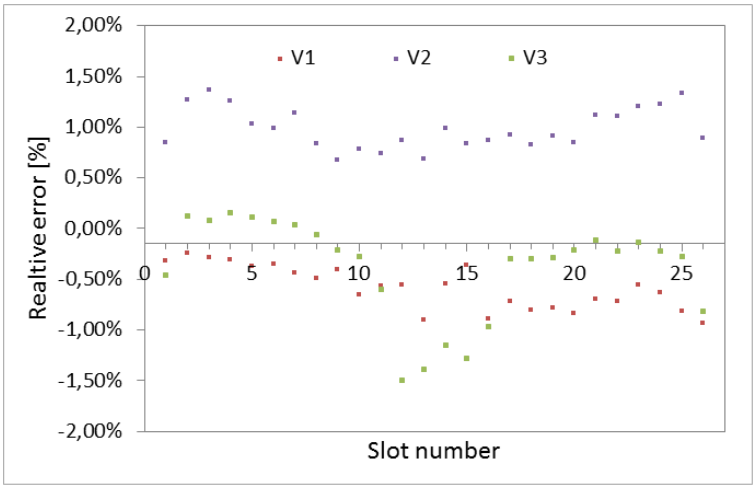

FIGURE A.2: Relative error of volume averaged coolant velocity in SbFP.

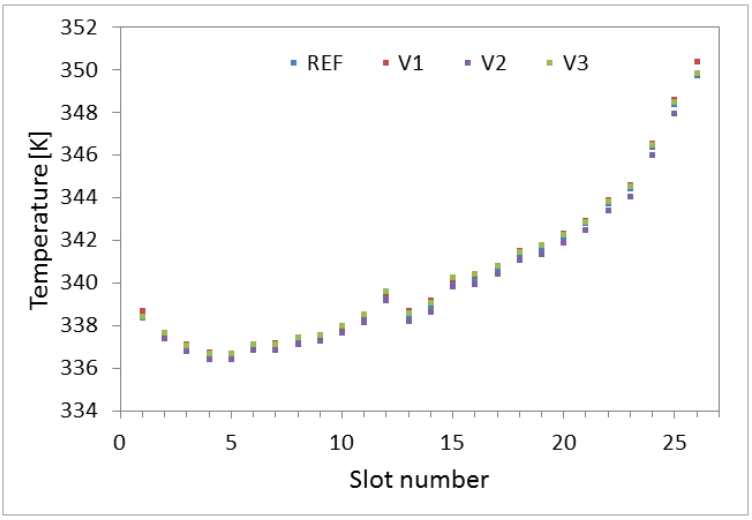

FIGURE A.3: Maximum temperature of SbFP wall.

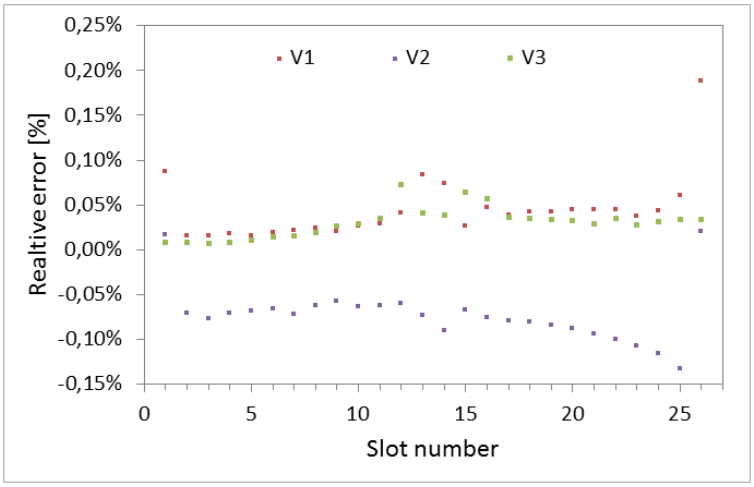

FIGURE A.4: Relative error o maximum temperature of SbFP wall.

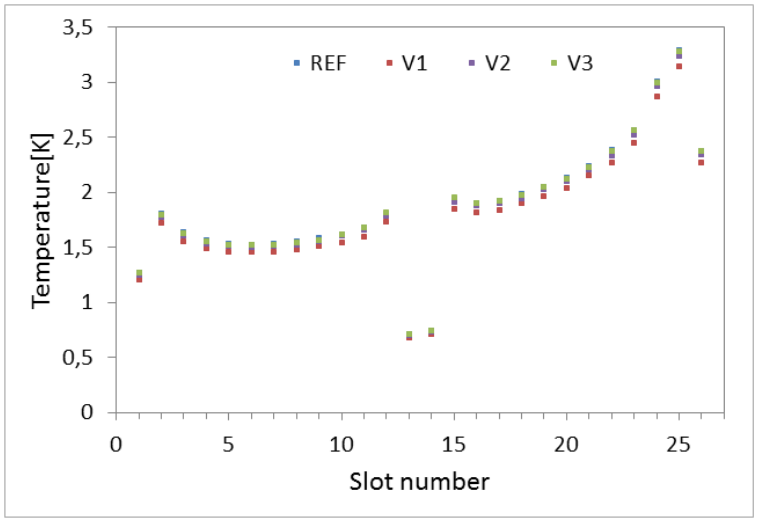

FIGURE A.5: Average coolant heat up in SbFP.

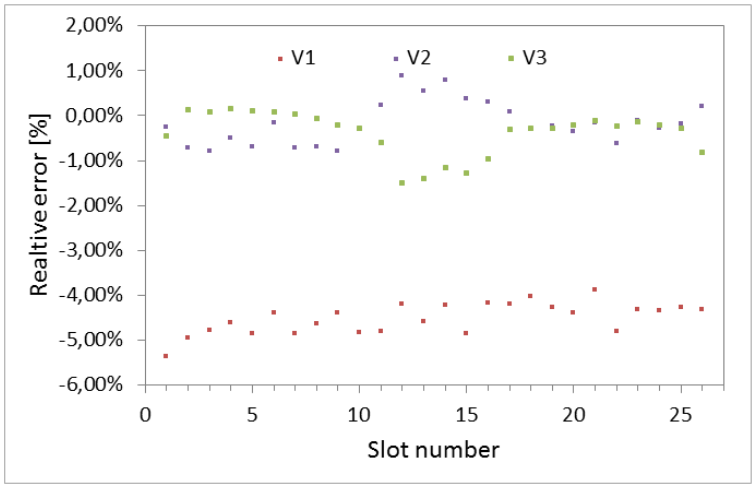

FIGURE A.6: Relative error of average coolant heat up in SbFP.

Since no major differences were observed and the errors fit below 5 per cent margin it can be stated that the solution are grid independent. However, one shall keep in mind that the boundary layer in estimated by the model for each of the discussed cases.

B Turbulence model verification

To verify if the results are independent from chosen turbulence model the reference case was calculated with SST k-ω model. The results are set in the charts presented in Figures B.3 - B.4. It can be observed that Realizable k-ϵ model underestimates values of coolant mass flow, velocity and the heat up, however it reaches higher values of maximum wall temperature. The differences between the results of the models are insignificant, thus the author decided to use Realizable k-epsilon model which gives slightly more pessimistic results to estimate possibly highest temperatures. For future works especially transient analysis both models shall be checked and compared since there are no specific guidelines which favour any on the model.

FIGURE B.1: Coolant mass flow rate with respect to the turbulence model.

FIGURE B.2: Coolant velocity with respect to the turbulence model.

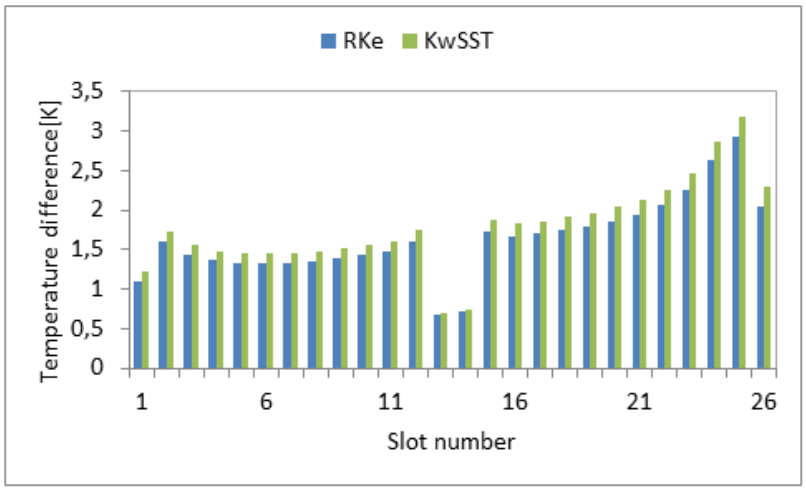

FIGURE B.3: Coolant heat up with respect to the turbulence model.

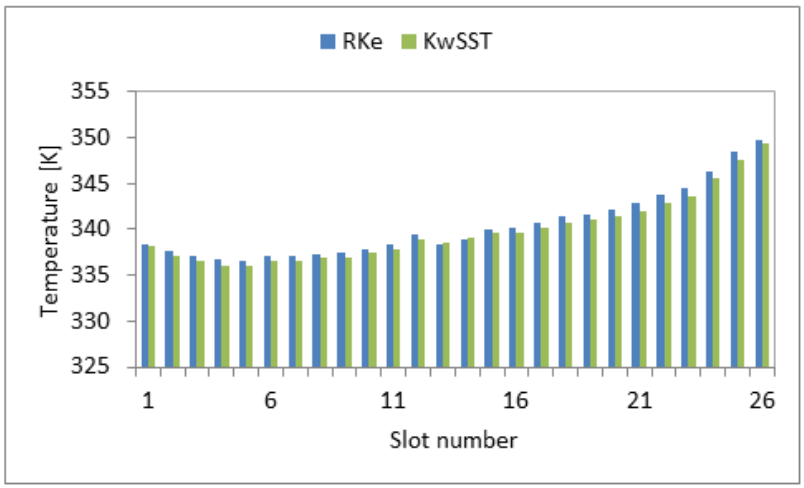

FIGURE B.4: Maximum wall temperature with respect to the turbulence model.

Bibliography

A. Gandhir, Y.Hassan (2011). "RANS modeling for flow in nuclear fuel bundle in pressurized water reactors (PWR)". In: *Nuclear Engineering and Design*.

Abu-Mulaweh, H.I. (2004). "Turbulent mixed convection flow over a forward-facing step - the effect of step heights". In: *International Journal of Thermal Sciences*.

ANSYS (2016a). *ANSYS Fluent Theory Guide, Release 17.2*. Tech. rep. ANSYS Inc.

— (2016b). *ANSYS Fluent User's Guide, Release 17.2*. Tech. rep. ANSYS Inc.

A.S. Alzwayi, M.C. Paul (2013). "Effect of width and temperature of a vertical parallel plate channel on the transition of the developing thermal boundary layer". In: *International Journal of Heat and Mass Transfer*.

A.Sh. Kherbeet M.R. Safei, H.A. Mohammed B.H. Salman H.E. Ahmed O.A. Alawi M.T. Al-Asadi (2016). "Heat transfer and fluid flow over microscale backward and forward facing step: A review". In: *International Communications in Heat and Mass Transfer*.

B.E.Launder, D.B.Spalding (1974). "The numerical computation of turbulent flows". In: *Computer Methods in Applied Mechanics and Engineering*.

Boyd, C. (2016). "Perspectives on CFD analysis in nuclear reactor regulation". In: *Nuclear Engineering and Design*.

Bykowski, B.A. Żarnecka-Bareja w. (1996). *Charakterystyka hydrauliczna pierwotnego obiegu chłodzenia basenu reaktora Maria*. Internal report Nr: B-13-96.

C.C. Liu Y.M. Ferng, C.K. Shih (2012). "C evaluation of turbulence models for flow simulation of the fuel rod bundle with a spacer assembly". In: *Applied Thermal Engineering*.

C.D. Argyropoulos, N.C. Markatos (2014). "Recent Advances on the numerical modelling of turbulent flows". In: *Applied Mathematical Modelling*.

Cengel, Y.A. (2012). *Heat Transfer. A Practical Approach. Second Edition.* Springer.

D. Bestion A. Martin, F. Menter M.Boucker S. Pigny M. Scheuerer M. Heitsch U. Rohde S. Willemsen H. Paillère D. Sweet M. Andreani (2004). *Recommendation on Use of CFD Codes for Nuclear Reactor Safety Analysis*.

D.G. Jehad G.A.Hashim, A.Kadhim Nor Azwadi Che Sidik (2015). "Numerical Study of Turbulent Flow over Backward-Facing Step with Different Turbulence Models". In: *Journal of Advanced Research Design*.

G.Hansen, S. Owen (2008). "Mesh generation technology for nuclear reactor simulation:barriers and opportunities". In: *Nuclear Engineering and Design*.

H. Koivunoroa E. Hippeläinena, I. Auterinenc L. Kankaanrantad M. Kulvike J. Laaksof T. Seppäläd S. Savolainena b H. Joensuud (2015). "Biokinetic analysis of tissue

boron(10B) concentrations of glioma patients treated with BNCT in Finland". In: *Applied Radiation and Isotopes*.

H .Rief R.van Heusden, G.Perlini (1993). "Generating epithermal neutron beams for neutron capture therapy in TRIGA reactors." In: *Advances in Neutron Capture Therapy*. Plenum Press.

IAEA-TECDOC-1223 (2001). *Current Status of neutron capture therapy*. Tech. rep. International Atomic Energy Agency.

J. Mahaffy B. Chung, F. Dubois F. Durcos E. Graffard M. Heitsh M. Henriksson E. Komen F. Moretti T. Morii P. Mühlbauer U. Rohde M. Scheuerer B.L. Smith C.Song T. Watanabe G. Zigh (2014). *Best Practices Guidelines for the use of CFD in nuclear reactor safety applications*. Tech. rep. OECD.

J.C. Lane, R.I. Loehrke (1980). "Leading Edge Separation From a Blunt Plate at Low Reynolds Number". In: *Transactions of the ASME*.

J.E. Jaramillo C.D. Perez-Segarra, A. Oliva K. Claramunt (2007). "Analysis of different RANS models applied to turbulent forced convection". In: *International Journal of Heat and Mass Transfer*.

J.R. Lamarsh, A.J. Baratta (2001). *Introduction to Nuclear Engineering. Third Edition.* Prentice Hall.

K. Pytel, et.al (2015). *Eksploatacyjny Raport Bezpieczenstwa Reaktora MARIA*. Tech. rep. Narodowe Centrum Badan Jadrowych.

K. Pytel W. Mieleszczenko, M. Dorosz T. Kulikowska Z. Marcinkowska (2010). *Safety Analyses of BNCT converter*. Internal Report.

K.E. Forster, R. Greif (1959). "Heat Transfer to a Boiling Liquid-Mechanism and Correlations". In: *Journal of Heat Transfer*.

Krzysztoszek, G. (2013). *Experience and Characteristics of Maria RR for material testing irradiation*. Tech. rep. IAEA.

— (2016). *The Characteristics and Irradiation Capabilities of MARIA Research Reactor in NCBJ Swierk*. Book of Abstract MINOS Conference.

M. Abdollahzadeh M. Esmaeilpour, R. Vizinho A. Younesi J.C. Pascoa (2017). "Assesment of RANS turbulence models for numerical study of laminar-turbulent transition in convection heat transfer". In: *International Journal of Heat and Mass Transfer*.

Wall Y^+ approach for dealing with turbulent flow over a surface mounted cube: Part 1 - Low Reynolds Number (2009a).

Wall Y^+ approach for dealing with turbulent flow over a surface mounted cube: Part 2 - High Reynolds Number (2009b).

M. Yaghoubi, S. Mahmoodi (2004). "Experimental Study of turbulent separated and reattached flow over a finite blunt plate". In: *Experimental Thermal and Fluid Science*.

M.A. Gryzinski M. Maciak, M. Wielgosz (2015). "Summary of recent BNCT Polish programme and future plans". In: *Applied Radiation and Isotopes*.

Madland, D.G. (2006). "Total prompt energy release in the neutron-induced fission of 235U, 238U, and 239Pu". In: *Nuclear Physics.*

Mentner, F.R. (1994). "Two-Equation Eddy-Viscosity Turbulence Models for Engineering Applications". In: *AiAA Journal*.

Flow separation characterization of a forward facing step immersed in a turbulent boundary layer (2009).

O.K. Harling K.L. Riley, T.H. Newton B.A. Wilson J.A. Bernard L-W. Hu E.J. Fonteneau P.T. Menadier S.J. Ali B. Sutharsan G.E. Kohse Y. Ostrovsky P.W. Stahle P.J. Binns W.S. Kiger III P.M. Busse (2002). "The fission converter based epithermal neutron irradiation facility at the Massachusetts Institute of Technology reactor." In: *Nuclear Science and Engineering*.

P.A. Prusinski S. Potempski, M. Borysiewicz K.Kowal T. Kwiatkowski A.M. Prusinski (2012). "CFD analysis of the safety related thermal hydraulic parameters describing a flow domain of an experimental medical installation (BNCT converter) inside of the Research Reactor MARIA". In: *Journal of Power Technologies*.

Prokopowicz, R. (2013). "Diagnostyka neutronowa w reaktorze jądrowym i termojądrowym z wykorzystaniem metody aktywacyjnej". PhD thesis. National Centre for Nuclear Research, Institute of Plasma Physics and Laser Microfusion.

T. Jinyuan H.Y. Guan, L.Chaoqun (2006). *Computational Fluid Dynamics: A practical Approach.* Butterworth-Heinemann.

Tarchalski, M. (2016). "Nuclear heating in the Maria Reactor and implementation of neutron and photon calculation scheme". PhD thesis. National Centre for Nuclear Research, AIX Marseille University.

Tracz, G. (2007). "Wtórne źródła neutronowe do generowania specyficznech strumieni neutronów". PhD thesis. Instytut Fizyki Jądrowej PAN.

Wierzchnicka, M. (2008). *Konwerter Uranowy*. Technical project Nr.M423-0 (org.Projekt techniczny).

Wilcox, D.C. (1988). *Turbulence Modeling for CFD*.

Z.Chen X-N. Chen, A. Rineiski P. Zhao H. Chen (2015). "Coupling a CFD code with neutron kinetics and pin thermal models for nuclear reactor safety analyses". In: *Annals of Nuclear Energy*.